B978-0-12-374452-4.00005-2, 00005

Chapter 5

c0005 # Pseudotachylytes and Earthquake Source Mechanics

Giulio Di Toro
Dipartimento di Geoscienze, Università di Padova, Italy
Istituto Nazionale di Geofisica e Vulcanologia, Rome, Italy

Giorgio Pennacchioni
Dipartimento di Geoscienze, Università di Padova, Italy
Istituto Nazionale di Geofisica e Vulcanologia, Rome, Italy

Stefan Nielsen
Istituto Nazionale di Geofisica e Vulcanologia, Rome, Italy

Destructive earthquakes nucleate at depth (10 to 15 km), therefore monitoring active faults at the Earth's surface, or interpreting seismic waves, yields only limited information on earthquake mechanics. Tectonic pseudotachylytes (solidified friction-induced melts) decorate some exhumed ancient faults and remain, up to now, the only fault rocks recognized as the unambiguous signature of seismic slip. It follows that pseudotachylyte-bearing fault networks might retain a wealth of information on seismic faulting and earthquake mechanics. In this chapter, we will show that in the case of large exposures of pseudotachylyte-bearing faults, as the glacier-polished outcrops in the Adamello massif (Southern Alps, Italy), we might constrain several earthquake source parameters by linking field studies with microstructural observations, high-velocity rock friction experiments, modeling of the shear heating and melt flow, and dynamic rupture models. In particular, it is possible to estimate the rupture directivity and the fault dynamic shear resistance. We conclude that the structural analysis of exhumed pseudotachylyte-bearing faults is a powerful tool for the reconstruction of the earthquake source mechanics, complementary to seismological investigations.

s0005 1. INTRODUCTION

p0010 Large earthquakes critical for human activities nucleate at ~7 to 15 km depth (*Scholz*, 2002). The sources of these earthquakes and the process of rupture propagation can be investigated by the geophysical monitoring of active faults from the Earth's surface or by the interpretation of seismic waves; most

B978-0-12-374452-4.00005-2, 00005

information on earthquake mechanics is retrieved from seismology (*Lee et al.*, 2002). However, these indirect techniques yield incomplete information on fundamental issues of earthquake mechanics (e.g., the dynamic fault strength and the energy budget of an earthquake during seismic slip remain unconstrained; *Kanamori and Brodsky*, 2004) and on the physical and chemical processes active during the seismic cycle.

p0015 To gain direct information on seismogenic sources, fault-drilling projects have been undertaken in several active faults, such as the Nojima Fault in Japan (*Boullier et al.*, 2001; *Ohtani et al.*, 2000), the Chelungpu Fault in Taiwan (*Ma et al.*, 2006), and the San Andreas Fault in the United States (*Hickman et al.*, 2004). Fault drilling allows integration of real-time *in situ* measurements (strain rate, pore pressure, etc.) and sampling with high-quality seismological data, collected by seismometers located at depth, and geodetic data at the surface (GPS, inSAR, etc.). However, fault drilling has several limitations: (1) to date, drilling is confined to shallow depths (<3 km); (2) the investigated fault volume is too small to provide representative 3D information on fracture networks and fault rock distribution (i.e., large earthquakes rupture faults with areas >100 km^2); and (3) the costs are high.

p0020 An alternative and complementary approach to gain direct information about earthquakes is the investigation of exhumed faults showing evidence of ancient seismic ruptures (a direct approach to the earthquake engine). However, the use of exhumed faults to constrain the mechanics of earthquakes also has limitations: (1) alteration during exhumation and weathering may erase the pristine coseismic features produced at depth; (2) reactivation of a fault zone by repeated seismic slip events may render it difficult or impossible to distinguish the contribution of individual ruptures; (3) single faults may record seismic and aseismic slip and there might be the need to distinguish between microstructures produced during the different stages of the seismic cycle (coseismic, postseismic, interseismic, etc.); (4) the microstructural proxies used to recognize the coseismic nature of a fault rock have not yet been identified with certainty except in some cases; and (5) the ambient (e.g., pressure, temperature) conditions and the stress tensor coeval with seismic faulting are often difficult to estimate with precision.

p0025 Therefore, the use of exhumed faults to retrieve information on earthquakes rely on (1) the recognition of faults rocks produced during seismic slip that have escaped significant structural overprinting and alteration until exhumation to the Earth's surface and (2) the presence of tight geological constraints that allow the determination of ambient conditions during seismic faulting. To date, the only fault rock recognized as a signature of an ancient earthquake is pseudotachylyte (*Cowan*, 1999). Pseudotachylyte is the result of solidification of friction-induced melt produced during seismic slip (*McKenzie and Brune*, 1972; *Sibson*, 1975; *Spray*, 1987, 1995). This chapter presents the study of an exceptional exposure of pseudotachylyte-bearing faults where many of the above-listed limitations are overcome. It will be

B978-0-12-374452-4.00005-2, 00005

shown that a multidisciplinary approach, which includes field and laboratory study of the natural pseudotachylytes integrated with theoretical and rock friction experiments, may yield fundamental information on earthquake mechanics and are complementary to seismological investigations. This new approach is inspired by the pioneering work of *Sibson* (1975). First we will briefly review the literature about pseudotachylytes, whose main geochemical, microstructural, and mesostructural features are summarized in detail by *Lin* (2007).

s0010 2. PSEUDOTACHYLYTES

p0030 The term *pseudotachylyte* was introduced by *Shand* (1916) to describe a dark, aphanitic, glassy-looking rock similar to basaltic glasses (or *tachylytes*: Shand in his 1916 paper used the wrong spelling, *tachylyte*, for the basaltic glass, or *tachilyte*. This resulted in the use of both the words pseudo*tachylyte* and pseudo*tachilyte* in the literature. In this paper, we will use the word introduced by Shand: *pseudotachylyte*) and filling networks and veins in the Old Granite of the Parijs region of the Vredefort Dome in South Africa. Pseudotachylytes have been found in numerous localities and different genetic environments within silicate-built rocks as impact structures (*Reimold*, 1998; *Shand*, 1916), "superfaults" (or large displacement faults related to the collapse of large structures as impact craters and calderas; *Spray*, 1997), rock landslides (*Lin et al*., 2001; *Masch et al*., 1985; *Scott and Drever*, 1953), pyroclastic flows (*Grunewald et al*., 2000), and faults (*Sibson*, 1975). The latter, referred to as tectonic pseudotachylytes, are the most common form, though considered rare between fault rocks by some authors (*Blenkinsop*, 2000; *Sibson and Toy*, 2006; *Snoke et al*., 1998). This chapter deals with tectonic pseudotachylytes.

p0035 Despite a long-lasting debate about the origin of tectonic pseudotachylytes (e.g., *Francis*, 1972; *Philpotts*, 1964; *Spray*, 1995; *Wenk*, 1978), they are now recognized as the product of comminution and friction-induced melting along a fault surface during seismic slip (i.e., at slip rates of 1 to 10 m s^{-1}). In fact, by definition pseudotachylyte is a fault rock that shows evidence of melting (*Magloughlin and Spray*, 1992). Although evidence for a quenching origin of pseudotachylytes has been occasionally reported in the literature since the beginning of the 20th century (*Holland*, 1900), *Scott Drever* (1953) described a vesicular glassy rock in a Himalayan Thrust (later recognized as the product of a large landslide; *Masch et al*., 1985), only in 1975 did *Sibson* show unambiguously from field evidence that frictional melting was possible during seismic faulting. From a theoretical point of view, *Jeffreys* (1942) demonstrated that friction-induced melting could occur along fault surfaces during coseismic slip. *McKenzie and Brune* (1972) investigated in detail the process of frictional melting and proposed that, given the stress conditions and the elevated strain rates achieved during seismic slip, frictional melting should be widespread in nature. *Wenk* (1978) later questioned the nature of

pseudotachylytes as quenched melts. He emphasized that few pseudotachylytes contain glass and suggested ultracomminution as the main mechanism responsible for the development of most fault rocks referred to as pseudotachylytes. Despite the fact that ultracomminution remains a valid alternative to frictional melting to explain the origin of some pseudotachylyte-looking fault rocks, a wealth of data has provided evidence that most of these fault rocks have indeed been through a melt phase (e.g., *Lin*, 1994; *Maddock*, 1983; *Shimamoto and Nagahama*, 1992). These data include field and microstructural observations as well as mineralogical, petrographical, and geochemical data (see Sections 2.1 and 2.2). In the lab, *Spray* (1987, 1988, 1995) clearly showed the origin of pseudotachylyte by frictional melting by using a frictional welding apparatus. In 1995, *Spray* demonstrated experimentally that grain size reduction during frictional sliding is a precursor of melting during coseismic slip: comminution and frictional melting are two related processes. In further experiments, *Tsutsumi and Shimamoto* (1997a) measured the evolution of the friction coefficient during sliding at high slip rates, showing that local melting and welding of the asperity contacts occurred before the bulk melting of the sliding surface. Thus, the comminution model proposed by *Wenk* (1978) was rejected. The lack of glass (often replaced by a cryptocrystalline matrix) in tectonic pseudotachylyte is explained by its instability in fault zones.

s0015 2.1. Mesoscale Geometry of Pseudotachylyte

p0040 Pseudotachylytes commonly occur in the field as sharply bounded veins associated with faults. The typical vein thickness is in the range of a few millimeters to several centimeters, though meter-thick veins are reported in some major faults (e.g., Outer Hebrides Thrust, *Sibson*, 1975; the Woodroffe Thrust, *Camacho et al*., 1995). The veins lay parallel to, and decorate discontinuously, the fault surface (fault veins, *Sibson*, 1975) or intrude the host rocks branching off the slip surface (injection veins, *Sibson*, 1975) (Figures 1a and 1b). Fault veins are interpreted to decorate the generation surfaces where frictional melt is produced during seismic slip and from where most of the melt is extruded to form injection veins. The latter are assumed to result from fracturing induced by fault pressurization due to thermal expansion during generation of the frictional melt (*Sibson*, 1975; *Swanson*, 1989, 1992). *Di Toro et al*. (2005a) proposed a complementary model for the production of injection veins, associated to the dynamics of propagation of an earthquake rupture.

p0045 Pseudotachylyte may occur in complex geometric arrangements including pseudotachylyte-cemented breccias, paired shears, duplexes, and side-wall ripouts (*Grocott*, 1981; *Swanson*, 1988, 1989, 2006). Contrasting geometries of the pseudotachylytes networks apparently develop as a function of the degree of host rock anisotropy (*Swanson*, 2006). Because seismic slip commonly occurs along preexisting planes of weakness, the geometry of precursor structures plays a major role in determining the architecture of pseudotachylyte networks.

B978-0-12-374452-4.00005-2, 00005

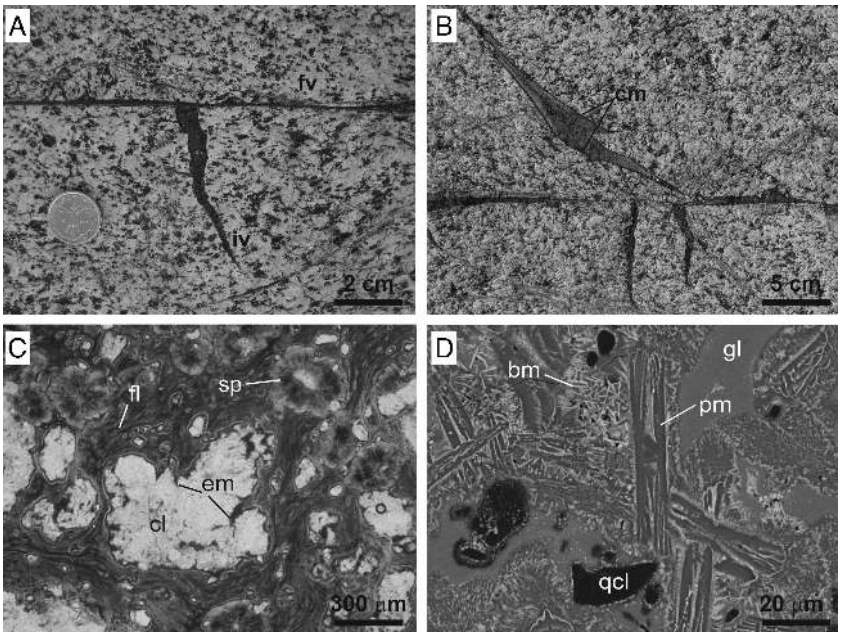

f0005 **FIGURE 1** Pseudotachylyte from the Gole Larghe Fault zone (Adamello, Italy). (a) Field image of a pseudotachylyte fault vein (fv) and an injection vein (iv) within the Avio tonalites. North is pointing downward. (b) Pseudotachylyte-bearing faults showing injection veins filling both fractures formed during coseismic slip (veins approximately orthogonal to the fault vein and intruding the block in the lower part of the photos) and fractures predating pseudotachylyte generation and associated with cataclastic faulting (vein oblique to the fault vein in the upper part of the photo) (see Section 4). Note the zoning (cm = chilled margin) in the latter vein (for microstructural description of chilled margins in these pseudotachylyte veins from the Gole Larghe Fault; see *Di Toro and Pennacchioni*, 2004). North is pointing downward. (c) Optical microstructures (plane-polarized light) of a pseudotachylyte. The pseudotachylyte consists of a brown cryptocrystalline matrix with flow structures (fl) and spherulites (sp) and including several clasts (cl). The matrix intrudes the clasts forming deep embayments (em). All these features, as discussed in Section 2.2, suggest that pseudotachylytes are solidified melts. (d) Back scatter scanning electron microscope image of the pseudotachylyte. Quartz clasts (qcl; black in color) are immersed in a fine matrix made of biotite microlites (bm; white), plagioclase microlites (pm; dark gray), and devitrified glass (gl; light gray).

s0020 2.2. Microstructures and Geochemistry in Pseudotachylytes

p0050 Pseudotachylytes consist of a microlitic to cryptocrystalline or glassy (more rare) matrix embedding survivor clasts of the host rock (Figures 1c and 1d). Several microstructures of pseudotachylyte matrix are identical or closely resemble microstructures of volcanic rocks (e.g., *Maddock*, 1983; *McPhie et al*., 1993) indicating rapid cooling of a melt. In fact, cooling to solidus temperature is in the range of a few seconds to minutes at seismogenic depths

(10–15 km) for typical pseudotachylytes (1 to 20 mm thick) (*Boullier et al.*, 2001; *Di Toro and Pennacchioni*, 2004). These microstructures include (1) microlites and spherulites with a wide variety of shapes (*Di Toro and Pennacchioni*, 2004; *Lin*, 1994, 2007; *Maddock*, 1983; *Magloughlin*, 1992; *Philpotts*, 1964; *Shimada et al.*, 2001) often arranged to define a symmetric zoning of the pseudotachylyte vein (chilled margin); (2) quenched sulfide droplets related to immiscibility in the silicate melt (*Magloughlin*, 1992, 2005); (3) vesicles and amygdales (*Maddock*, 1986; *Magloughlin*, 1992; *Scott and Drever*, 1953), and (4) flow structures (e.g., *Lin*, 1994) (Figures 1c and 1d). Glass has been reported rarely in pseudotachylytes (*Lin*, 1994; *Obata and Karato*, 1995; *Toyoshima*, 1990), which reflects its high instability under geological conditions, but pseudotachylytes may show secondary (devitrification) microstructures (*Lin*, 1994; *Maddock*, 1983).

p0055 Clasts within the pseudotachylyte include both single-mineral or lithic clasts from the host rock. Host rock minerals are not equally represented between the clasts mainly due to selective nonequilibrium melting of the different mineral species and, therefore, to preferential consumption of the low-melting point minerals (*Shand*, 1916; *Spray*, 1992). In many pseudotachylytes within granitoids, phyllosilicates and amphiboles are rare between clasts, whereas plagioclase and, especially, quartz tend to survive in the melt (*Di Toro and Pennacchioni*, 2004). The type of survivor clasts also depends on other physical properties of the mineral, such as fracture toughness and thermal conductivity (*Spray*, 1992). Clasts are angular to rounded and show embayment in the case of melting (*Magloughlin*, 1989). They commonly act as nuclei for the growth of radially arranged microlites of the same mineral species to develop spherulitic microstructures (*Di Toro and Pennacchioni*, 2004; *Shimada et al.*, 2001). The clast size distribution within pseudotachylytes is fractal in the clast size range of 10 to 2000 μm, with a fractal dimension D of about 2.5 (*Di Toro and Pennacchioni*, 2004; *Shimamoto and Nagahama*, 1992). The clast size distributions typically have a kink at grain size of about 5 μm and show "fractal" values $D < 2.5$ for the smaller grain fraction that is interpreted as due to the preferential assimilation of the finer-grained grains in the melt (*Ray*, 1999; *Shimamoto and Nagahama*, 1992; *Tsutsumi*, 1999). This observation is a further support for the origin of pseudotachylytes from a melt because comminution alone cannot explain the decrease in smaller grains (*Shimamoto and Nagahama*, 1992). Clasts smaller than 1 μm in size are uncommon in the pseudotachylyte matrix, probably in relation to "the critical limit at which the energy for melting becomes smaller than that for comminution" (*Wenk et al.*, 2000, p. 271; for a discussion, see also *Pittarello et al.*, 2008).

p0060 Because of the preferential melting of mafic minerals, the pseudotachylyte melts are commonly more mafic in composition than the host rock. This is the strongest evidence that disequilibrium (i.e., single mineral) melting, rather than eutectic melting, occurs during pseudotachylyte generation. Because of

B978-0-12-374452-4.00005-2, 00005

the presence of clasts within the matrix, geochemical studies on the matrix are usually done using microprobe analysis with a defocused beam (e.g., *Ermanovics et al*., 1972; *Spray*, 1988) or by subtracting the clast content from the bulk XRF (X-ray fluorenscence) composition (*Di Toro and Pennacchioni*, 2004; *Sibson*, 1975). Composition of the matrix has been compared with the composition of the associated fault rock (i.e., cataclasites; *Di Toro and Pennacchioni*, 2004; *Magloughlin*, 1992) or of the bounding rocks (e.g., *Maddock*, 1992). Several authors have described pseudotachylyte compositions related to disequilibrium partial melts (*Allen*, 1979; *Bossière*, 1991; *Camacho et al*., 1995; *Maddock*, 1986, 1992; *Magloughlin*, 1989; *Sibson*, 1975; *Spray*, 1992, 1993). *Philpotts* (1964) and later *Ermanovics et al*. (1972) showed near total melting of the host rock with the exception of quartz. *O'Hara and Sharp* (2001) used isotope composition to show the large contribution of biotite and K-feldspar and minor quartz in the production of frictional melt. Total melting of the fault rock assembly was proposed for pseudotachylyte associated with ultramafics (*Obata and Karato*, 1995) and mylonites (*Toyoshima*, 1990).

p0065 In summary, when a fault rock records several types of evidence from outcrop scale to microscale that suggest a melt origin, it can be called a pseudotachylyte (*Magloughlin and Spray*, 1992; *Passchier and Trouw*, 1996; *Reimold*, 1998). Among the structural evidence for a melt origin of pseudotachylytes, the foremost is the intrusive habit of injection veins and the presence of flow structures (*Sibson*, 1975). Second, pseudotachylyte veins often exhibit microlitic and spherulitic textures, chilled margins, or glass, indicating rapid chilling of a melt (*Lin*, 1994; *Maddock*, 1983). However, the presence of glass is not a necessary feature of these rocks, because the environmental conditions under which pseudotachylytes form (usually between 3 to 15 km in depth) are unfavorable for glass preservation (*Lin*, 1994; *Maddock*, 1986). Third, fractal analysis of size distribution of clasts in pseudotachylytes shows that the number of small grains (<5 micron) is very small compared to the number of larger grains. This is indicative of preferential melting of the finest clasts (*Shimamoto and Nagahama*, 1992). Lastly, frictional melting is a nonequilibrium process, with the consequence that pseudotachylytes usually contain survivor clasts of quartz and feldspar and the matrix is enriched in Fe, Mg, Al, Ca, and H_2O compared to the host rock or to the cataclastic precursor (*Sibson*, 1975).

s0025 2.3. Temperature Estimate of Frictional Melts

p0070 The value of peak temperature of the friction-induced melt is an important parameter to estimate the energy budget during seismic slip as well as on the lubricating effect of the melt (see Section 5.1). In natural pseudotachylytes, melt temperatures were deduced by different methods, including the following:

o0005 **1.** SiO_2 glass composition (T_{melt} 1450°C; *Lin*, 1994).

o0010 **2.** Microlite mineralogy ($T_{melt} = 890$ to 1100°C: two pyroxene geothermometer; *Toyoshima*, 1990; $T_{melt} = 790°$ to 820°C: omphacite-garnet

geothermometer; *Austrheim and Boundy*, 1994; $T_{melt} = 1000°C$: pigeonite crystallization; *Camacho et al*., 1995; $T_{melt} = 1200°C$, mullite crystallization, *Moecher and Brearley*, 2004).

o0015 **3.** Mineralogy of survivor clasts ($T_{melt} = 1000°C$; *Maddock*, 1983).

o0020 **4.** Numerical modeling by matching melt cooling curves with the presence of microlitic versus spherulitic zoning in thick veins assuming that the different microstructures are the result of contrasting cooling rates at the center and periphery of the pseudotachylyte vein ($T_{melt} = 1450°C$; *Di Toro and Pennacchioni*, 2004).

o0025 **5.** Volume ratio between lithic clasts and matrix (*O'Hara*, 2001).

p0100 In high-velocity rock friction experiments, melt temperatures of 1000° to 1550°C were measured by means of a radiation thermometer and thermocouples (*Del Gaudio et al*., 2006; *Hirose and Shimamoto*, 2005a; *Lin and Shimamoto*, 1998; *Spray*, 2005; *Tsutsumi and Shimamoto*, 1997b). In summary, the estimates and measures of the temperature of melts in natural and experimental pseudotachylytes are in the range of 750° to 1550°C. Given the fact that pseudotachylyte is often hosted in granitoids or in rock with a silica-rich composition, these temperature estimates support the idea that friction-induced melts are produced by nonequilibrium melting (*Spray*, 1992) and that they are superheated (*Di Toro and Pennacchioni*, 2004). In fact, the equilibrium melting temperature for granitoid systems ranges between 700° and 850°C (*Philpotts*, 1990). However, most temperature estimates and measures probably underestimate the peak temperature achieved by the melt. For instance, microlite mineralogy yields a cooling temperature. In experiments, the radiation thermometer measures the temperature over a spot size of 400 μm in diameter, whereas the slipping zone thickness measured at the end of the experiment is ~180 μm thick only (*Del Gaudio et al*., 2006). It follows that the measured temperature is an average between that of the wall rocks and the slipping zone. Thermocouples, inserted in the specimen, measure the temperature inside the sample and not in the slipping zone, and the temperature of the melt is estimated through numerical modeling refinement (*Tsutsumi and Shimamoto*, 1997b). Because some pseudotachylytes record melting microstructures of quartz and apatite (e.g., embayed clasts), temperatures as high as 1700°C can be locally achieved if disequilibrium melting and H_2O-free conditions (in the case of quartz melting) are assumed. Together with frictional melting, a possible mechanism for melt superheating is viscous shear heating in the melt layer (*Nielsen et al*., 2008).

s0030 2.4. Distribution of Tectonic Pseudotachylytes

p0105 Most pseudotachylytes are clearly linked to brittle (elastico-frictional, Sibson, 1977) and are associated with cataclasites (e.g., *Di Toro and Pennacchioni*, 2004; *Fabbri et al*., 2000; *Magloughlin*, 1992) or fluidized gouge (*Otsuki*

B978-0-12-374452-4.00005-2, 00005

et al., 2003; *Rowe et al*., 2005). Other pseudotachylytes, instead, appear closely linked to ductile (quasi-plastic, Sibson, 1977) regimes because they overprint and are in turn reworked by ductile shear zones (*Passchier*, 1982; *Sibson*, 1980; *White*, 1996). These latter pseudotachylytes are found associated with greenschist facies mylonites (*Passchier*, 1982; *Takagi et al*., 2000), amphibolite facies mylonites (*Passchier*, 1982; *Pennacchioni and Cesare*, 1997; *White*, 1996), granulitic facies mylonites (*Clarke and Norman*, 1993), and spinel-lherzolite facies mylonites (*Ueda et al*., 2008). Thus, pseudotachylytes are produced both at shallow (2 to 10 km) and midcrustal levels (10 to 20 km). Pseudotachylytes can be produced during intermediate and deep earthquakes also, but probably by processes other than frictional melting (we will not describe these mechanisms here). Eclogitic facies pseudotachylytes (> 60 km in depth) were found in the Bergen Arc of Western Norway (*Austrheim and Boundy*, 1994). The production of frictional melts (and plasmas) was invoked for the deep focus (637 km in depth) 1994 Bolivian mantle earthquake (M_w 8.3) (*Kanamori et al*., 1998).

s0035 2.5. Production of Pseudotachylytes

p0110 In this chapter, we focus on the mechanism of pseudotachylyte production in the elastico-frictional continental crust (<12 to 15 km depth for a geothermal gradient of 25°C km^{-1}, *Sibson*, 1977). During rupture propagation and coseismic slip (e.g., Figure 2a), the elastic energy stored in the wall rock is released (*Reid*, 1910). Part of the released elastic energy is dissipated in frictional work W_f on the fault. We may assume that W_f is partitioned in (*Kostrov and Das*, 1988)

$$W_f = Q + U_s \tag{1}$$

p0115 where Q is heat and U_s is surface energy for gouge and fracture formation (see Table 1 for a list of symbols used in this chapter). Because U_s is considered negligible (*Lockner and Okubo*, 1983), most (>95%) of the work done in faulting is converted to heat (*Scholz*, 2002, p. 155), especially in the lower part of the elastico-frictional crust (e.g., 10 km depth, *Pittarello et al*., 2008). It follows that the amount of heat generated during seismic slip for unit area of the fault is (*Price and Cosgrove*, 1990)

$$W_f = \mu(\sigma - p_p)d \approx Q \tag{2}$$

p0120 where μ is the friction coefficient, σ is the normal stress, p_p is the pore fluid pressure, and d is the coseismic slip. The heat flux generated per unit area of the fault is (*McKenzie and Brune*, 1972)

$$q \approx \mu(\sigma - p_p)V \tag{3}$$

p0125 where V is the slip rate.

p0130 The thermal penetration distance x in the bounding host rock as a function of slip duration t is

$$x \sim (\kappa\, t)^{0.5} \tag{4}$$

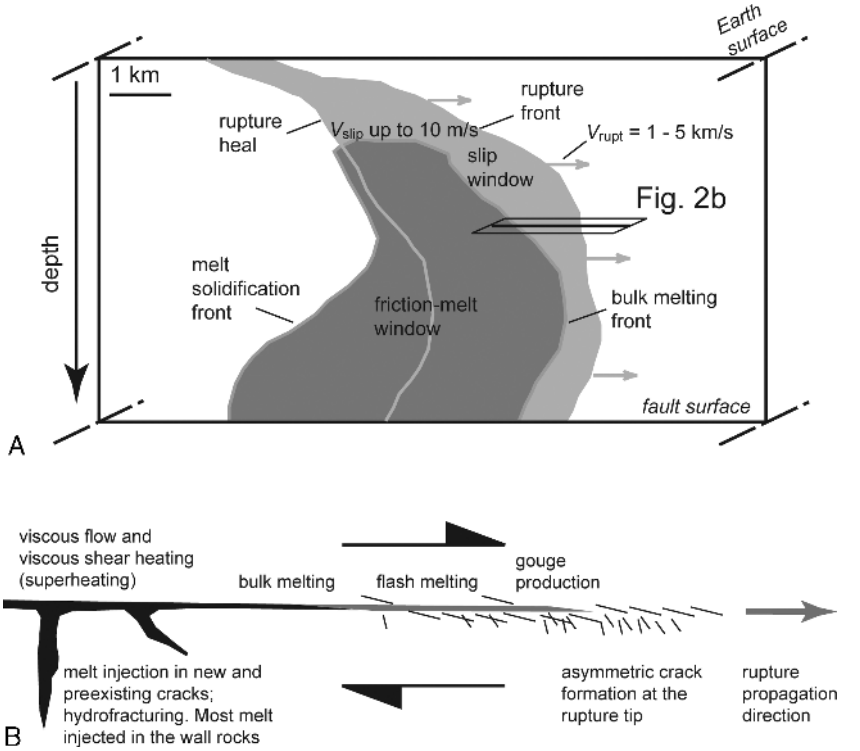

f0010 **FIGURE 2** Schematic models of pseudotachylytes production (modified from *Swanson*, 1992). (a) Model of propagation of a seismic self-healing pulse mode II crack. The fracture propagates toward the right side (as indicated by the gray arrows) at a speed V_{rupt} in the range between 1 and 5 km/s. Behind the rupture front, slip is restricted to a band (light gray area, in large part overlapped by the dark gray area of presence of friction melts). The slipping area is a few km wide. As the slipping area moves behind the fracture front, friction melt is produced after some refinement along the fault plane and may survive for some time (friction-melt window) after the cessation of slip. (b) Enlargement of the rupture along the fault section shown in Figure 2a. The rupture propagates to the right and the sense of shear is dextral. The stress perturbation induced by the propagation of the crack produces fractures in the lower block under tensional transient stress (see Section 4). Gouge production and comminution at the rupture tip are followed by flash melting (i.e., melting at asperity contacts) and bulk melting. Wall rocks interaction and viscous shear heating in the melt layer allow the achievement of extremely high temperatures (superheated frictional melts; see Section 5). Most melt is injected in the wall rocks.

p0135 where κ is thermal diffusivity of the host rock. The heat produced is large even for small slips (Equation 3) (*Sibson and Toy*, 2006) given (1) the high effective stress in the seismic source area (hundreds of MPa at depths in the range of 2 to 15 km) and (2) the high particle velocities (1 to 10 m s^{-1}) localized in thin slipping zones (few mm at most; *Sibson*, 2003). *McKenzie and Brune* (1972) estimated that melting could occur for fault slips as small as 1 to 3 mm for driving stresses of 100 MPa, and production of seismic melts

B978-0-12-374452-4.00005-2, 00005

t0005 **TABLE 1 Latin and Greek Symbols**

Latin Symbols	
A	Fault surface area (m^2)
c_p	Solid specific heat at constant pressure ($J\ K^{-1}\ kg^{-1}$)
c_{pm}	Melt specific heat at constant pressure ($J\ K^{-1}\ kg^{-1}$)
d	Displacement (m)
E	Heat (J)
E_m	Total energy input for unit mass ($J\ kg^{-1}$)
H	Latent heat of fusion ($J\ kg^{-1}$)
L	Effective latent heat of fusion ($J\ kg^{-1}$)
L_e	Dimension related to the escaping distance of the frictional melt from the sliding surface
N_f	Normalizing factor ($Pa^{0.75}$)
p_p	Pore pressure (MPa)
q	Heat flux per unit area ($J\ m^{-2}\ s^{-1}$)
Q	Heat density ($J\ m^{-2}$)
r	Specimen radius (m)
r_1	Specimen inner radius (m)
r_2	Specimen outer radius (m)
R	Revolution rate of the motor (s^{-1})
t	Time (s)
T_c	Characteristic temperature (K)
T_m	Rock melting temperature (K)
T_M	Maximum temperature achieved by the melt (K)
T_{hr}	Host rock temperature (K)
U_s	Surface energy for gouge and surface formation ($J\ m^{-2}$)
V	Slip rate ($m\ s^{-1}$)
V_e	Equivalent slip rate ($m\ s^{-1}$)
V_{Ray}	Rayleigh rupture propagation velocity, about 90% of V_{shear} ($m\ s^{-1}$)
V_{rupt}	Rupture propagation velocity ($m\ s^{-1}$)
V_{shear}	Shear wave velocity ($m\ s^{-1}$)

Continued

TABLE 1 Latin and Greek Symbols – (Cont'd)

Latin Symbols	
w	Melt half thickness (m)
w_{av}	Slipping zone average thickness (m)
W	Factor with velocity dimensions (m s^{-1})
W_f	Frictional work density done in faulting (J m^{-2})
x	Thermal penetration distance (m)
Greek Symbols	
$\dot{\varepsilon}$	Shear rate (s^{-1})
η_c	Characteristic viscosity (Pa s)
η_e	Equivalent viscosity (Pa s)
κ	Solid thermal diffusivity (m^2 s^{-1})
κ_m	Melt thermal diffusivity (m^2 s^{-1})
μ	Coefficient of friction
ν	Shortening rate (m s^{-1})
ρ	Solid density (kg m^{-3})
ρ_m	Melt density (kg m^{-3})
σ	Normal stress (MPa)
τ	Shear stress (MPa)
τ_p	Peak shear stress (MPa)
τ_{ss}	Steady-state shear stress (MPa)
ϕ	Ratio between the volume of lithic clasts and the total volume of pseudotachylyte
ω	Rotary speed (s^{-1})

for such small slips is confirmed by field evidence (*Griffith et al.*, 2008). Because of the low value of κ in crustal rocks (10^{-6} m^2 s^{-1}) and the short duration of seismic slip at a point of a fault (few seconds at most), heat remains *in situ* and the process is adiabatic at seismogenic depths (see *Di Toro et al.*, 2006b, for a detailed discussion). Given these deformation conditions, fault rocks as well as the host rocks immediately adjacent to the slipping surface are heated and eventually melt (e.g., *Bizzarri and Cocco*, 2006; *Fialko*, 2004; *Nielsen et al.*, 2008).

B978-0-12-374452-4.00005-2, 00005

p0140 A possible scenario for frictional melt production in the elastico-frictional crust is shown in Figure 2 (modified from *Swanson*, 1992). Unstable sliding occurs due to the velocity weakening behavior of most of the rock materials (i.e., friction coefficient decreases with increasing sliding speed; e.g., *Tullis*, 1988) and the rupture propagates as a mode II self-healing (*Heaton*, 1990) pulse (Figure 2a). At the rupture tip (Figure 2b), the stress perturbation during crack propagation induces fracturing in the wall rock under tension (the southern block for a rupture propagating toward the east along a dextral strike-slip fault; see Section 4). The opposite sliding surfaces are then uncoupled and a cushion of gouge develops in between during sliding. Rupture propagation is followed by surface refinement through crushing, clast rotation, and flash heating and melting (*Archard*, 1958; *Rempel*, 2006; *Rice*, 2006) of the initiation gouge. Bulk melting occurs where the gouge is highly comminuted and strain rate is higher, though it mainly involves the minerals with the lowest melting point (see Sections 2.2 and 2.3) (Figure 2b). With increasing slip, the opposite surfaces are separated by a thin layer of melt, which is further heated due to viscous shear heating (superheated melts). Melting occurs at the wall rocks for rock-rock interaction and for phase transition at the melt-wall rock and melt-survivor clast boundaries (*Nielsen et al*., 2008). The melt produced in the slipping zone (i.e., the fault vein) is mostly injected in the wall rocks, along (1) prerupture fractures (if the rupture is propagating along a preexisting fault) and (2) new fractures produced under the dynamic transient stress field at the rupture tip during propagation and due to the volume increase related to the melting of the rock. The melt is largely dragged and injected in the wall rocks, but a small percentage of melt still remains along the slipping zone. Under these conditions, the fault is lubricated by friction melts (*Nielsen et al*., 2008). Once the elastic strain energy stored in the wall rocks that drives the propagation of the rupture is released, the slip rate drops down, and the viscous strength of the melt layer increases instantaneously (see Section 5), leading to the healing of the rupture. This process may occur in 1 to 10 s at most, consistent with rise times typical of earthquakes. Instead, the melt injected into the wall rocks or pounding in dilational jogs along the fault vein (i.e., reservoirs), cools slowly, from seconds to minutes, depending on the peak temperature of the melt, the temperature of the host rock, and the thickness of the melt layer: melt might be still present after the healing of the rupture (friction melt window in Figure 2a). The solidification of the melt produces the pseudotachylyte.

s0040 2.5.1. The Role of Water

p0145 The role and the origin of water during frictional melting is still debated (*Allen*, 1979; *Magloughlin*, 1992; *Magloughlin and Spray*, 1992; *O'Hara and Sharp*, 2001; *Sibson*, 1973, 1975). The presence of fluid inclusions, vesicles, and amygdales in some pseudotachylyte (*Boullier et al*., 2001; *Maddock*

B978-0-12-374452-4.00005-2, 00005

et al., 1987; *Magloughlin*, 1992; *Obata and Karato*, 1995; *Philpotts*, 1964) suggests that water fluids must be present at the time of pseudotachylyte generation in some cases. However, it is not clear if water was present as pore water before frictional heating or, instead, if it was released by the breakdown of water-bearing minerals (biotite, chlorite, epidote, amphibole, etc.) during frictional heating (e.g., *Moecher and Sharp*, 2004). The presence of pore water in a slipping zone should impede the achievement of high temperatures, because (1) fluid expansion promoted by frictional heating induces a drastic decrease in the effective normal stress and lubricates the fault (*Allen*, 1979; *Bizzarri and Cocco*, 2006; *Lachenbruch*, 1980; *Mase and Smith*, 1987; *Rice*, 2006; *Sibson*, 1973), (2) water vaporization adsorbs heat, and (3) the expulsion of hot fluids cools the slipping zone. It follows that pseudotachylytes have been commonly assumed to develop in relatively dry rocks (*Sibson*, 1973; *Sibson and Toy*, 2006). On the other hand, water-rich conditions may also promote the production of pseudotachylytes by lowering the rock and mineral melting temperatures (*Allen*, 1979; *Magloughlin*, 1992). Recent field observations support the occurrence of frictional melting under fluid-rich conditions in some cases (*Rowe et al*., 2005; *Ujiie et al*., 2007). *Okamoto et al.* (2006) described pseudotachylytes bounded by a carbonate-matrix implosion breccia in the Shimanto accretionary complex (Japan). In this water-rich environment, during seismic slip, frictional heating expanded the pore water (thermal pressurization) in the slipping zone. Thermal pressurization induced (1) fracturing in the wall rocks, (2) expulsion of pressurized water, and (3) carbonate precipitation. Expulsion of pressurized water increased the effective stress (and temperature) leading to frictional melting in the slipping zone (*Okamoto et al*., 2006). In other words, frictional melting occurred *after* the expulsion of water from the slipping zone during the same seismic rupture.

s0045 3. A NATURAL LABORATORY OF AN EXHUMED SEISMOGENIC SOURCE

p0150 A few studied outcrops have suitable characteristics (large exposures, polished surfaces, presence of pseudotachylytes) that allow a wealth of information about earthquake mechanics to be retrieved from exhumed faults. Examples of such outcrops are from the Outer Hebrides Thrust (Scotland; *Sibson*, 1975), the Homestake Shear Zone (Colorado; *Allen*, 2005), the Fort Foster Brittle Zone (Maine; *Swanson,* 1988, 1989, 2006), and the Woodroffe Thrust (Australia; *Camacho et al*., 1995). In this chapter we will describe an exceptional outcrop of the Gole Larghe Fault zone (Southern Alps, Italy) (*Di Toro and Pennacchioni*, 2004, 2005; *Di Toro et al*., 2005a, 2005b, 2006b; *Pennacchioni et al*., 2006).

p0155 The Gole Larghe Fault zone is a dextral strike-slip exhumed structure crosscutting the Adamello tonalites (Italian Alps) and forming a southern branch of the Tonale line (a segment of the Periadriatic Lineament, the major

B978-0-12-374452-4.00005-2, 00005

fault system of the Alps; *Schmid et al.*, 1989) (Figure 3a). The Gole Larghe Fault zone is exposed in large glacier-polished unweathered outcrops, which allow a 3D investigation of the structures (Figure 3b) and where single faults can be mapped in detail (Figures 3c and 3d). The fault zone hosts a large number of pseudotachylytes, which have largely escaped alteration and structural reworking during the exhumation to the Earth's surface and therefore preserve an intact record of the coseismic processes that occurred at depth. In addition, the numerous pseudotachylytes present along the different faults are "simple" (a single continuous layer of melt): each pseudotachylyte layer records a single coseismic slip. At the same time, the fault zone contains hundreds of

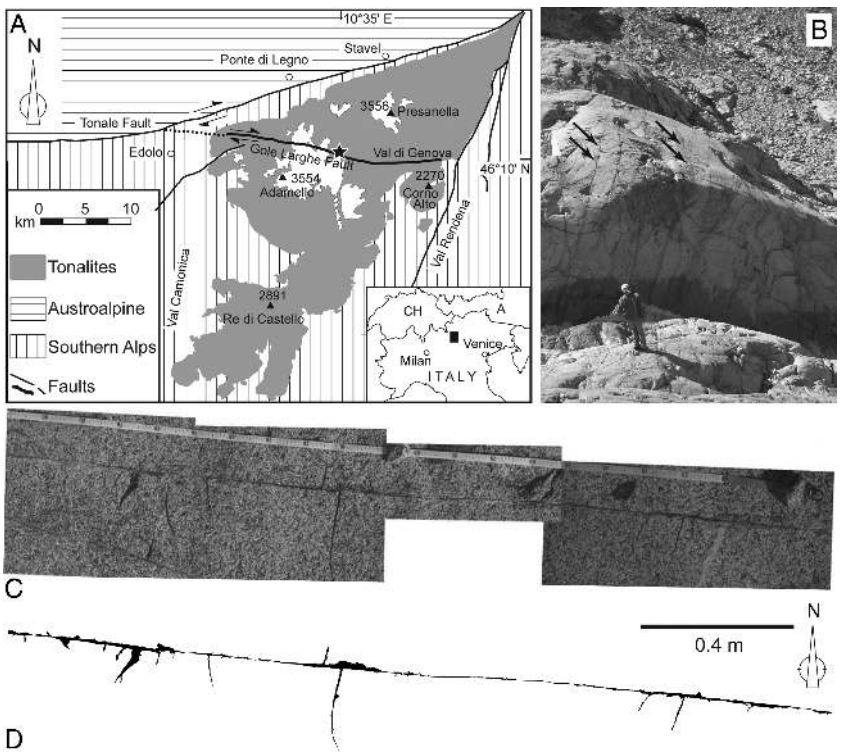

f0015 **FIGURE 3** A natural laboratory of a seismogenic fault zone: the Gole Larghe Fault zone in the Adamello batholith (Italy). (a) Tectonic sketch map of the Adamello region showing the location of the Gole Larghe Fault and of the glaciated outcrops (star) analyzed in detail in this contribution. (b) Field view of the exposures of the Gole Larghe Fault zone. Presence of deep creeks allows a 3D view of the fault zone. The fault zone is made of about 200 subparallel strike-slip faults (some indicated by arrows). (c) Photomosaic showing a pseudotachylyte-bearing fault zone. The excellent exposure allows the detailed mapping of the pseudotachylyte vein network and the precise estimate of the melt volume (area) per unit fault length. (d) Drawing of the pseudotachylytes from the photomosaic of Figure 3c. The orientation of the fractures filled by pseudotachylyte was used to reconstruct the seismic rupture directivity (see Section 4.2).

faults, which possibly record different seismic slip increments thus forming a statistically representative population of earthquakes occurring under identical ambient conditions and geological context. The outcrops contain numerous markers (aplite dikes, basic enclaves) crosscut by the faults, which allow the offset to be estimated for each single structure, whereas the host rock (tonalite) is homogeneous over kilometers along the fault. Numerous researchers have investigated the geology of the area since the 1950s, and there are tight constraints on the age and ambient conditions of deformation. All of the features make this fault an exceptional and rather unique natural laboratory for the direct study of an exhumed segment of a seismic zone (the earthquake engine).

p0160 The Gole Larghe Fault zone is exposed for a length of about 12 km in the northern part of the Adamello batholith within the tonalites of the Avio pluton (Figure 3a). The Avio tonalites consist of plagioclase (48% in volume), quartz (29%), biotite (17%), and K-feldspar (6%) (*Di Toro and Pennacchioni*, 2005), and are dated at 34 Ma (*Del Moro et al.*, 1983). In the upper Genova Valley (star in Figure 3a), the fault zone is 550 m thick and accommodates about 1 km of slip (*Di Toro and Pennacchioni*, 2005; *Pennacchioni et al.*, 2006). The fault zone includes hundreds of subparallel faults striking east-west, and mostly steeply dipping (50° to 80°) to the south, showing a spacing on the range of decimeters to a few meters (some shown in Figure 3b). The presence of subhorizontal roof pendants sunk in the Adamello batholith suggests that the batholith and the fault zone were not tilted during exhumation (*Callegari and Brack*, 2002). The faults exploit a main set of east-west trending joints pervasively developed in the whole intrusion. Fault surfaces have shallowly plunging (toward W) slickenlines and the marker offset indicates right-lateral strike-slip kinematics (*Di Toro and Pennacchioni*, 2005). Major faults accommodate up to 20 m of slip and are spaced every ~10 m, whereas the minor faults in between accommodate offsets of a few decimeters to a few meters. These subparallel faults are associated with a network of small fault-fractures produced during slip on the major and minor faults (*Di Toro and Pennacchioni*, 2005).

p0165 Fault rocks are cataclasites and pseudotachylytes. The Gole Larghe cataclasites are cohesive fault rocks cemented by the pervasive precipitation of epidote, K-feldspar, and minor chlorite due to fluid-rock interaction along the faults (*Di Toro and Pennacchioni*, 2005). These epidote- and K-feldspar-bearing fault rocks are referred to as cataclasites in the following text. Typically, pseudotachylyte is associated with the last event of slip recorded by each fault segment; pseudotachylyte overprints cataclasite (*Di Toro and Pennacchioni*, 2005). This sequence of events possibly results from the fact that (1) grain size reduction by cataclasis promotes successive melting (e.g., *Spray*, 1995) and (2) quenching of the friction-induced melts welds the fault and favors migration of successive slip events to other subparallel cataclastic faults. This interpretation is consistent with experimental observations: samples containing an artificially generated pseudotachylyte (produced by former

B978-0-12-374452-4.00005-2, 00005

high-speed frictional experiments with precut samples) break along the "intact" sample rather than along the welded surfaces (*Hirose and Di Toro*, unpublished data). This indicates that the fault recovers mechanical properties similar to that of the intact rock after sealing off by pseudotachylyte. In the Gole Larghe Fault zone, the welding process of individual faults by pseudotachylyte formation determines the progressive thickening of the fault zone and results in a low displacement/thickness ratio of the fault zone. This is in stark contrast with what occurs in many mature faults where repeated seismic ruptures localize along the same weak horizons and result in high displacement/fault thickness ratio (e.g., *Chester et al*., 1993).

p0170 Ar-Ar stepwise dating of the Adamello pseudotachylytes yields ages of ~30 Ma (*Pennacchioni et al*., 2006), indicating that seismic slip along the Gole Larghe was contemporary to the activity of the Tonale Fault (*Stipp et al*., 2002). Pseudotachylytes were produced only 3 to 4 Ma after the emplacement of the pluton. Zircon and apatite fission track data (*Stipp et al*., 2004; *Viola et al*., 2001) and other geological constraints indicate that faulting in the Adamello occurred after cooling of the pluton at the ambient conditions of 0.25 to 0.35 GPa (corresponding approximately to 9 to 11 km depth) and 250° to 300°C before the uplift of the batholith (*Di Toro and Pennacchioni*, 2004; *Di Toro et al*., 2005b; *Pennacchioni et al*., 2006). Therefore, the Gole Larghe pseudotachylytes record events of seismic slip that occurred at the base of the elastico-frictional (brittle) crust.

p0175 A main drawback at using the Gole Larghe faults to determine mechanical parameters of a single earthquake is that, in many faults, it is not possible to partition the fault slip between the cataclastic and the coseismic, pseudotachylyte-producing slip (*Di Toro et al*., 2005b). However, a few fault segments of the Gole Larghe Fault contain only pseudotachylytes and record a single seismic rupture of intact tonalite (*Di Toro et al*., 2006a; see Section 5.1). The absence of an epidote- and K-feldspar-bearing cataclasite precursor in these fault segments was determined by both field and microstructural observations (*Pittarello et al*., 2008). Note that rock fragmentation *during* seismic slip is a precursor to frictional melting (*Spray*, 1995) and is part of the *same* seismic rupture that produces the pseudotachylyte (see Figure 2b and Equation 1), but the epidote-bearing cataclasites were produced during a *different* deformation event with respect to the pseudotachylytes (i.e., not the same seismic rupture; see *Di Toro and Pennacchioni*, 2005, for field and microstructural evidence).

p0180 A further difficulty to study earthquake mechanics by the use of exhumed faults is that information is needed about the effective stress tensor at the time of seismic slip. In the Adamello faults, the orientation of principal axis of stress is relatively well constrained by regional and field structural data (*Mittempergher et al*., 2007; *Pennacchioni et al*., 2006). The maximum compressive stress is approximately horizontal and nearly at 45° to the faults and the stress field can be reasonably assumed as Andersonian (*Di Toro et al*., 2005b). The widespread production of pseudotachylytes constrains the pore

fluid pressure to hydrostatic or less (*Sibson*, 1973). The friction coefficient at rupture was assumed of 0.75 given the high segmentation of the precursor joints (which involves, in some places, the propagation of the seismic rupture in an intact tonalite) and the pervasive cementation of fault segments by indurated, precursor, cataclasites (*Di Toro and Pennacchioni*, 2005). Given these assumptions, we estimated, for subvertical faults at 10 km depth, a normal stress to the fault ranging between 112 and 184 MPa, and a resolved shear stress ranging between 84 and 138 MPa (*Di Toro et al*., 2005b, 2006b). Au1

p0185 Though the structure, fault rock mineral assemblage, and geochemical composition are identical over 12 km along strike of the Gole Larghe Fault zone (i.e., *Pennacchioni et al*., 2006), we focused our attention on the outcrops located at the base of the Lobbia glacier because of their excellent exposure (star in Figure 3a). The results described in the following sections were obtained from this area.

s0050 4. RUPTURE DYNAMICS

p0190 As discussed in Section 2, the presence of pseudotachylyte on exhumed faults is a clear marker of seismic activity. In addition, some of the damage structures are not only involved in the seismic process but are ostensibly of coseismic genesis, in particular, freshly fractured fault branches and lateral fractures permeated with pseudotachylyte that are clearly not associated with any preexisting regional or local deformation trend (e.g., Figure 2b). As a consequence, those coseismically generated structures may be identified as markers of the aggressive dynamic stress transient associated with fast rupture propagation (and, eventually, of the associated fluid pressure and temperature surges). The pattern, distribution, and the intensity of the stress transient associated with fracture propagation are specific of dynamic conditions, namely fracture length, velocity, propagation direction, stress drop, energy dissipation during fracturing, and extension of the weakening process zone at the crack tip (where slip weakening occurs). Therefore, any measurable feature (position, orientation, opening) of the coseismic structures on an exhumed fault is a potential gauge allowing the properties of the paleo-earthquake source to be constrained and characterized, with implications for present-day earthquakes under a similar context. In the following section, some salient features of the fracture transient stress will be illustrated, henceforth related to the marker structures observed in the field, and, finally, used to reconstruct features of the associated earthquake source.

s0055 4.1. Transient Stress Pattern

p0195 Both static and dynamic cracks embedded in an elastic medium, subjected to a remotely applied load, induce a perturbation of the stress field in the surrounding medium. Whereas the pattern associated with a static crack only

B978-0-12-374452-4.00005-2, 00005

depends on the slip distribution inside the crack itself, the pattern associated with a dynamically propagating fracture will also critically depend on its tip propagation velocity relative to the wave velocity in the surrounding medium. The differences between static and dynamic fracturing will become significant when the fracture is moving at a substantial fraction of the medium's sound velocity. A determining feature is the stress concentration located at or in the vicinity of the propagating tip, where the yielding strength of the rock is reached and a finite energy flow allows the dissipative process of fracture propagation to occur (*Irwin*, 1957). Some of the simplest mathematical models, assuming cracks with infinitely sharp tips, involve the idea that stress diverges to infinity at the fracture termination (*Kostrov*, 1964). Such a feature is obviously an unphysical consequence of a simplistic mathematical model; however, even more realistic models where the crack tip is allowed to spread over a finite process region or "end zone" (*Ida*, 1972) predict that the stress concentration at the fracture termination can be pronounced. This feature is compatible (1) with the observation of profuse damage observed in the vicinity of crack extremities (*Rice*, 1966) and (2) with the necessity of finite energy flow within a relatively small region around the tip to allow for fracture propagation (*Irwin*, 1957). Theory predicts that, for a fixed amount of energy dissipated in the propagation of fracture, the length of the end zone at the fracture tip collapses as its propagation velocity increases, tending to zero as the velocity approaches its limiting velocity (either the shear or Rayleigh wave velocity of the medium, depending on the configuration). Such a process is analogous to the Lorentz contraction observed in relativistic physics (*Burridge et al*., 1979). Therefore, spreading of the tip is reduced and the stress concentration tends to reproduce a quasi-singular stress distribution, in agreement with that of the sharp tip mathematical model. Under such circumstances, the perturbation relative to the background stress is much more localized and intense for a crack propagating close to its limiting velocity. Recent crack models take into consideration the dissipative process not only on the crack surface itself but also in a finite volume around the slip zone and in the vicinity of the propagating tip (where the large stress transient stress is attained) (*Andrews*, 2005). Through such a mechanism, the end zone is not subjected to the shrinking effect discussed earlier; the dissipation increases with crack propagation and is distributed over a wider volume, whereas the stress concentration remains bounded.

s0060 4.2. Examples of Transient Stress Markers Observed

p0200 Markers of transient stress have been described in numerical simulations, laboratory tests, and even in one instance on natural faults, the case of the paleoseismic faults of the Gole Larghe (*Di Toro et al*., 2005a).

p0205 Because rocks and most materials are weaker in tension than in compression, secondary fractures are expected to be produced in the block under

B978-0-12-374452-4.00005-2, 00005

tension (e.g., *Andrews*, 2005). This theoretical prediction is confirmed by experiments conducted in photoelastic rock analog materials (homalite). *Samudrala et al*. (2002) fired bullets on a sample assemblage made of a precut homalite sheet glued along a preexisting interface (Figure 4a). The bullet triggered eastward propagation of the crack, dextral slip along the precut surface, and formation of secondary fractures on the sample side experiencing tensile transient stresses (Figure 4b). Though these experiments were performed under no confinement, it can be shown that a state of absolute tension can be reached during dynamic fracturing even under the lithostatic loads expected at seismogenic depth (*Griffith et al*., 2008).

p0210 In the field example of the Gole Larghe faults, a series of coseismic, secondary fractures was observed to branch from the main faults (Figure 4c). Assuming that the geometry of the observed paleoseismic faults is almost that of a purely vertical, strike-slip fault, and considering a horizontal section through the fault plane, the geometry may be reduced for simplicity to that of an in-plane (mode II) fracture. In this case, the limiting velocity in the subshear wave case is V_{Ray} (the Rayleigh wave velocity, in general slightly above 90% of the shear wave velocity). As the fracture propagation approaches V_{Ray}, it can be shown that the transient stress perturbations around the propagating fracture are exacerbated, eventually inducing tension sufficient to surpass the lithostatic load at the estimated depth at the time of activity (10 km) and allowing the opening of tension cracks. A rotation of the axis of major tension and compression also occurs; the angle of principal

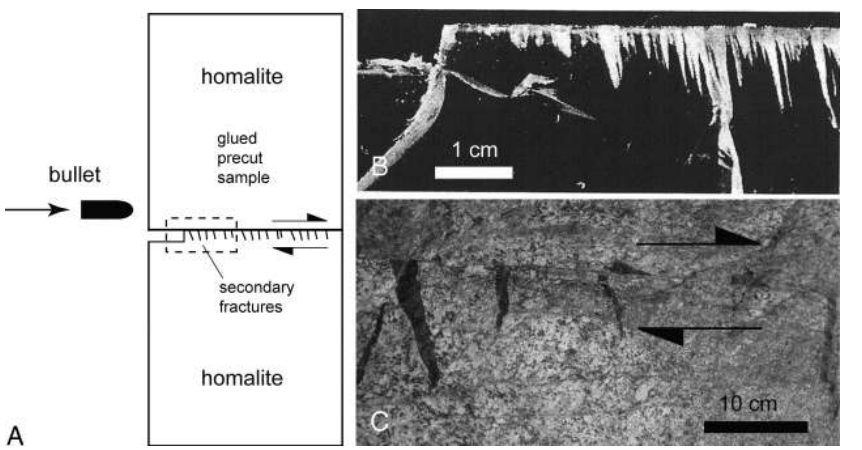

f0020 **FIGURE 4** Markers of transient stress: field and experimental results. (a) A description of the experimental setup, where a dynamic fracture is triggered by shooting a bullet onto a homalite sample (modified from *Samudrala et al*., 2002). (b) The results of the same experiment, with secondary branching cracks on the side where tensile transient stress is produced. (c) An example of exhumed seismic fault (*Di Toro et al*., 2005a), where the lateral branching cracks are found in majority on one side and in a dominant direction, yielding constraints on rupture directivity and rupture velocity (see the text for further details).

B978-0-12-374452-4.00005-2, 00005

compressive stress initially at 30° to the fault plane progressively increases until reaching a maximum of about 90° as the fracture velocity increases and approaches V_{Ray}. The location of tension is always on the side of the fault where slip is in the direction opposite to fracture propagation, whereas compression is observed on the other side. Accordingly, the presence of open (mode I) pseudotachylyte-filled cracks branching off mainly in the southern wall of the Gole Larghe Faults at roughly 90° (Figure 4c), given that the slip motion was dextral, indicates that rupture was propagating from the east to the west. In addition, to reach absolute tensional conditions at 90°, the fracture velocity ought to be close to V_{Ray}.

p0215 Branching fractures were filled by pseudotachylyte (e.g., Figures 3c and 4c), confirming that they were produced or opened during the propagation of the seismic rupture. In particular, of 624 fractures filled by pseudotachylyte and measured over a length of 2 to 10 m in 28 different subparallel fault segments, 67.7% intruded the southern bounding block (i.e., the veins injecting into the southern block are more than 70% on 17 fault segments, 60% to 70% on three segments, 50% to 60% on five segments, and less than 50% in only three fault segments) (Figure 5a). The angle of the fracture, measured clockwise starting from the east, had two dominant orientations, at about 30° to 210° (set 1) and 90° to 270° (set 2) with respect to the fault trace (*Di Toro et al.*, 2005a). Set 1 fractures intruded preexisting cataclastic faults, whereas set 2 fractures were produced during rupture propagation along the main fault surface.

p0220 The stress perturbations induced by the propagation of the rupture during the 30 Ma old Gole Larghe earthquakes were investigated by means of numerical models (Figures 5b, 5c, and 5d). In these models were considered different coseismic slips (up to 1.5 m, consistent with displacements measured in the field; see Figure 6), rupture propagation modes (crack-like versus self-healing pulses, the latter of 0.1 to 1 km in length—according to the self-healing pulse model, the slipping region is much smaller than the final dimension of the earthquake), stress drops, and slip weakening distances. Because the dynamic stress field, given a fixed prestress direction, depends on the ratio of the rupture propagation velocity V_{rupt} with the shear wave velocity V_{shear}, the simulation considered slow rupture velocities ($V_{rupt} = 0.6\ V_{shear}$), typical of large dissipation in the fracture process; high rupture velocities ($V_{rupt} = 0.9\ V_{shear}$), about 98% of the Rayleigh wave velocity, commonly reported for many earthquakes; and supershear rupture velocities ($V_{rupt} = \sqrt{2}V_{shear}$), estimated for some large earthquakes (*Bouchon and Vallée*, 2003). In the case of subsonic rupture velocities ($V_{rupt} < V_{shear}$; Figure 5b), an analytical solution was used, whereas a finite difference solution was used in the case of supersonic rupture speeds (Figure 5d). In the model, the properties of the tonalite were used (Poisson ratio of 0.25, shear modulus of 26 GPa, fracture toughness of 2 MPa $m^{0.5}$, rock density of 2700 kg m^{-3}). Whatever the combination of rupture speed and crack mode, the rupture tip was under tension in the southern block for right-lateral faults propagating from the west to the east (consistently with the experimental results shown in Figure 4b). However, by varying

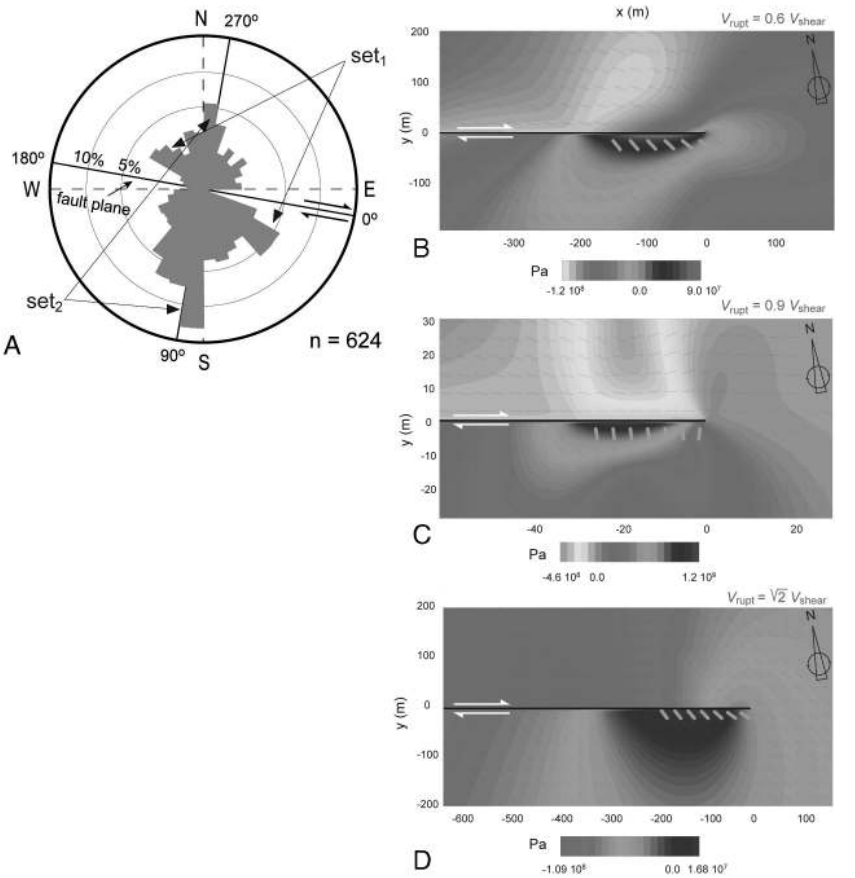

f0025 **FIGURE 5** (a) Area-weighted rose diagram showing the orientation of the injection veins filled by pseudotachylyte from 28 fault segments of the Gole Larghe Fault zone. The fractures are measured clockwise from the east side of the fault (see Figure 3c). Most fractures are toward the south and oriented at about 30° and 85° from the main fault. (b-d) Numerical models of the tensile stress field (positive is tension, negative compression) close to the rupture tip for three different rupture velocities (b: $V_{rupt} = 0.6\ V_{shear}$; c: $V_{rupt} = 0.9\ V_{shear}$; d: $V_{rupt} = \sqrt{2}V_{shear}$). The fracture tip is shown as a black thick line and viewed from above. The fault is dextral, the rupture is propagating eastward and the wall rocks are under tension in the southern side in all models. The planes of maximum tensile stress are indicated by thin black segments: the planes in the southern side and near to the rupture tip are evidenced in orange. For $V_{rupt} = 0.9\ V_{shear}$ (Figure 3c), the planes of maximum tension are oriented at about 85° from the main fault, consistently with the most common orientation of the fractures observed in the Gole Larghe Fault. All figures are from *Di Toro et al.* (2005a). **(See Color Plate 14)**.

the rupture velocity, the magnitude of the stresses varied and the orientation of the planes of maximum tension rotated. In particular, for V_{rupt} approaching the V_{Ray} (i.e., about 0.9 V_{shear}, Figure 5c), the solutions yielded the highest values of tensional stress (up to 1.7 GPa, well above the strength under

B978-0-12-374452-4.00005-2, 00005

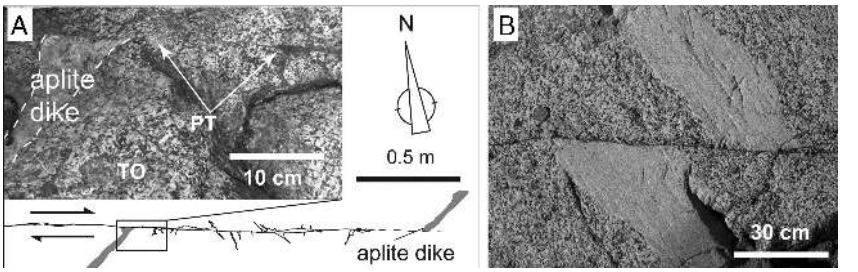

f0030 **FIGURE 6** Estimate of dynamic fault strength from field exposures. (a) Fault segment, decorated by (only) pseudotachylyte, separating an aplite dike of about 1.5 m. Most pseudotachylyte is injected in the wall rocks, and pseudotachylyte fault vein thickness is variable along strike. In this case, the pseudotachylyte "thickness" w_{av} appearing in Equation 12 was estimated as the ratio between the pseudotachylyte area in outcrop and the length of the fault segment. (b) Aplite dike is crosscut at an offset of about 30 cm by a fault segment decorated by only pseudotachylyte. The fault displacement was estimated by the measures of the marker separation and of the orientation of the fault, outcrop, marker, and slickenlines (*Di Toro and Pennacchioni*, 2005).

tension for granite, which is about 20 MPa) and an orientation of the planes under maximum tension consistent (80° to 90°) with the most frequent orientation of tensional fractures (injection veins) measured in the field. Some injection veins intrude the northern wall and could be the result of nonplanar geometry of the fault, fracturing due to the volume increase related to the melting of tonalite and cataclasite (about 17%), or some rupture complexities like the interaction of neighbor fault segments. The stress drop associated with the modeled rupture is 42 MPa, which is consistent with the expected stress drop related to the lubrication effects of the frictional melt (see Sections 5 and 6). The estimated fracture energy (the energy dissipated during the propagation of the crack) is between 8 and 67 MJ m^{-2}. As a consequence, fieldwork and numerical modeling suggest eastward propagation of the seismic ruptures at Rayleigh wave velocities. Because the Gole Larghe Fault is a dextral branch of the Tonale Fault, which was active at 30 Ma, and the structure, mineralogy, and geochemistry of the fault zone are identical along the whole length of the fault, the interpretation is that the Gole Larghe Fault zone records hundreds of ruptures propagating from the west (the Tonale Fault) to the east.

p0225 Large earthquakes (some fault segments in the Gole Larghe record coseismic slip of 1.5 m (see Figure 6a) which is compatible with M6-7 earthquakes; *Sibson*, 1989) occur over repeated times of the order of 100 to 1000 years (*Scholz*, 2002). A major advantage in using exhumed ancient faults compared to monitoring active faults is the possibility of investigating rupture directivity over the geological timescale and to produce a statistically robust database. The conclusion that some fault zone may record a dominant rupture directivity has implications in earthquake hazard evaluation. Indeed, the radiated wave field from a unilateral propagating rupture is amplified in the direction

of propagation (directivity effect) but reduced in the opposite direction, thus inducing increased strong motion in one direction and anisotropy in the potential distribution of damage.

s0065 5. DYNAMIC FAULT STRENGTH

p0230 The determination of the magnitude of the shear stress and traction acting on the fault surface during seismic slip is relevant in earthquake mechanics. For instance, the decrease in shear stress during seismic slip may determine (1) whether dynamic stress drop is larger than static stress drop (*Bouchon*, 1997), (2) the rupture propagation mode (e.g., self-healing pulse versus crack-like; *Beeler and Tullis*, 1996; *Heaton*, 1990; *Nielsen and Carlson*, 2000), (3) the increase in the ratio of radiated energy versus seismic moment with earthquake size (*Mayeda and Walter*, 1996), and (4) the production of heat during seismic slip (e.g., *Lachenbruch*, 1980). However, fault strength during seismic slip cannot be retrieved through seismological methods except for particular cases (*Guatteri and Spudich*, 1998, 2000). In fact, extrapolation from seismic waves may allow the estimate of the static stress drop (*Hanks*, 1977)—and, by means of strong assumptions, of the dynamic stress drop (*Bouchon*, 1997)—but not the absolute values of the shear stress (*Scholz*, 2002).

p0235 Experiments conducted with the "conventional" biaxial and triaxial apparatuses (*Lockner and Beeler*, 2002) at slip rates <1 mm/s and slip <1 cm (orders of magnitude lower than seismic deformation conditions) show that rock friction ($\mu = \tau/\sigma$ where τ is shear stress and σ is normal stress to the fault) is about 0.7 in most cohesive and noncohesive rocks (*Byerlee*, 1978) over a large range of temperatures (almost up to 400°C in the case of granite; *Stesky et al.*, 1974) and pressures (up to 2 GPa; *Byerlee*, 1978). Exceptions to Byerlee's law are some clay minerals and phyllosilicates (montmorillonite, talc, vermiculite) showing lower friction values. The "conventional" experiments also show that the friction coefficient is slightly perturbed (few percentage points at most) by variations in slip rate (velocity weakening) and increasing displacement (slip weakening) (*Marone*, 1998; *Scholz*, 2002; *Tullis*, 1988). The evolution of the μ with slip rate and displacement is described by the Dieterich-Ruina rate and state (R&S) friction law (*Dieterich*, 1978, 1979; *Ruina*, 1983), which has found a broad application in earthquake mechanics (from rupture dynamics to aftershock physics; see *Scholz*, 1998, for a review). However, the R&S friction law was formulated to describe experimental results obtained under deformation conditions significantly different from the seismic ones and is not capable of accounting for some seismological observations such as those listed in points 1 through 4, presented earlier. To explain these observations, several fault-weakening mechanisms were proposed, including thermal pressurization (*Sibson*, 1973), normal interface vibrations (*Brune et al.*, 1993), acoustic fluidization (*Melosh*, 1996), elastohydrodynamic lubrication (*Brodsky and*

B978-0-12-374452-4.00005-2, 00005

Kanamori, 2001), silica gel lubrication (*Di Toro et al*., 2004; *Goldsby and Tullis*, 2002), thermal decomposition (*Han et al*., 2007), flash heating at asperity contacts (*Rempel*, 2006; *Rice*, 2006), gouge-related weakening (*Chambon et al*., 2002; *Mizoguchi et al*., 2007), and melt lubrication (*Spray*, 1993). Among these, experimental evidence was given for silica gel lubrication (*Di Toro et al*., 2004; *Goldsby and Tullis*, 2002), thermal decomposition (*Han et al*., 2007), gouge-related weakening (*Mizoguchi et al*., 2007), and melt lubrication (*Di Toro et al*., 2006a; *Spray*, 2005). However, because these weakening mechanisms have been found very recently in the laboratory, their occurrence in nature and their physics remain almost unknown (*Beeler*, 2006). The exception is melt lubrication. Artificial pseudotachylytes were produced in high-velocity friction experiments in the late 1980s (*Spray*, 1987), and their mechanical properties were investigated from the late 1990s (*Tsutsumi and Shimamoto*, 1997a). Noteworthy, pseudotachylytes (solidified melts) exist in natural exhumed faults and are similar to artificial pseudotachylytes (*Di Toro et al*., 2006a; *Spray*, 1995). Then, the physics of melt lubrication of faults has been studied with some detail (*Fialko and Khazan*, 2005; *Nielsen et al*., 2008). Lastly, it is possible to estimate the dynamic shear stress during seismic slip from the amount of melt produced (*Sibson*, 1975). As a consequence and different from the other weakening mechanisms proposed so far, in the presence of pseudotachylyte it is possible to extrapolate experimental results to natural conditions and validate if there is any weakening effect on fault strength at seismic slip rates. As shown in the next sections, field, experimental, and theoretical work suggests that faults are lubricated by seismic melts.

s0070 5.1. Field Estimates

p0240 *Sibson* (1975) and *Wenk et al*. (2000) suggested estimating the average dynamic shear stress in pseudotachylyte-bearing faults by assuming that all the frictional work during seismic slip is converted to heat (i.e., the process is fully adiabatic) and that the energy expended to produce new surfaces is negligible. Actually, both assumptions are probably valid at 10 km depth (*Di Toro et al*., 2006b; *Lockner and Okubo*, 1983; *Pittarello et al*., 2008). From Section 2.5 we note:

$$W_f \approx Q \tag{5}$$

p0245 That is, most frictional work during sliding results in fault rock heating and, eventually, in melting (*Jeffreys*, 1942; *McKenzie and Brune*, 1972). The total energy E_m input for unit mass (J kg^{-1}) is partitioned in (1) energy exchanged for rock heating until melting ($c_p\,(T_m - T_{hr})$), (2) energy exchanged during rock melting (H), and (3) energy required for further melt heating ($c_{pm}\,(T_M - T_m)$) if frictional melts are superheated (*Di Toro and Pennacchioni*, 2004; *Fialko and Khazan*, 2005; *Nielsen et al*., 2008):

$$E_m = c_p(T_m - T_{hr}) + H + c_{pm}(T_M - T_m) \tag{6}$$

where T_m is the rock melting temperature, T_{hr} is the ambient host rock temperature, T_M is the maximum temperature achieved by the melt, H is the latent heat of fusion, and c_p and c_{pm} are the specific heat (J K^{-1} kg^{-1}) at constant pressure of the solid phase and of the melt, respectively. In the case of frictional melts, because of the presence of survivor clasts in the matrix that do not exchange latent heat of fusion, Equation 6 becomes

$$E_m = c_p(T_m - T_{hr}) + (1-\phi)H + (1-\phi)c_{pm}(T_M - T_m) + \phi)c_p(T_M - T_m) \tag{7}$$

where ϕ is ratio between the volume of lithic clasts and the total volume of pseudotachylyte (i.e., matrix + lithic clasts). Then, assuming that $c_{pm}(T) \approx c_p(T)$:

$$E_m \approx (1-\phi)H + c_p(T_M - T_{hr}) \tag{8}$$

and the energy input E (J) is:

$$E \approx [(1-\phi)H + c_p(T_M - T_{hr})]\rho\ A\ W_{av} \tag{9}$$

where ρ is the density (assuming melt density approximately equal to rock density), A is the area of the fault surface, and w_{av} is the average width of friction-induced melt present as veins along the fault plane. The work for unit area (J m^{-2}) done to overcome the frictional sliding resistance for a constant τ_f is

$$W_f = d\ \tau_f \tag{10}$$

where d is the coseismic fault displacement. W_f is converted to heat E. Considering the area of the fault surface where frictional work occurs, from Equations 8, 9, and 10,

$$E \approx E_m\ \rho\ A\ w_{av} \approx d\ \tau_f A \tag{11}$$

and the average τ_f is

$$\tau_f \approx \rho\ E_m\ w_{av}/d \approx \rho[(1-\phi)H + c_p(T_M - T_{hr})]\ w_{av}/d \tag{12}$$

p0280 In the case of the Gole Larghe Faults zone, all the variables in Equation 9 can be determined for pseudotachylyte-bearing faults formed in intact tonalite (i.e., without a precursor, preseismic, cataclasite), and it is possible to estimate the average dynamic shear stress during seismic faulting. The values for $c_p \approx 1200$ J kg^{-1} K^{-1}, $H = 3.24 \times 10^5$ J kg^{-1}, and $\rho = 2700$ kg m^{-3} are known from the literature (*Di Toro et al.*, 2005a, and references therein). The ambient host rock temperature of $T_{hr} \sim 250°C$ is well constrained by geological data, microstructural observations, and the mineralogy of cataclasite coeval with pseudotachylyte production and seismic faulting (*Di Toro and Pennacchioni*, 2004). The peak temperature of the friction-induced melt was

B978-0-12-374452-4.00005-2, 00005

>1200°C, as indicated by the crystallization of plagioclase microlites with andesine composition and the assimilation of plagioclase clasts, and it was estimated at 1450°C based on numerical modeling of microlitic-spherulitic zoned distribution in pseudotachylyte veins (*Di Toro and Pennacchioni*, 2004). A value $\phi = 0.2$ was determined by means of image analysis of scanning electron microscope images of the pseudotachylyte veins (*Di Toro and Pennacchioni*, 2004). These values yield $E_m = 1.7 \times 10^6$ J kg^{-1} from Equation 8. The ratio w_{av}/d was determined in fault segments where field and microstructural (SEM, FE-SEM) investigations revealed that the pseudotachylyte layer and seismic slip were produced during a single slip event (i.e., there was no evidence of alteration or precursor cataclasite) and rupture propagated through an intact rock (Figure 6). In the case of thin fault veins, the thickness was measured directly in the field (Figure 6a). In the case of thicker and more complicated pseudotachylyte veins filling larger displacement fault segments, the average thickness was determined from fault profiles (intersection of the fault with the outcrop surface) obtained from photomosaics of the fault (Figures 3c, 3d, and 6b). The average thickness w_{av} was calculated as the area of the pseudotachylyte (including the melt injected in the host rock) divided by the length of the fault profile. The coseismic slip d was determined from separations of dikes. From Equation 12, the calculated dynamic shear stress was in the range between 14.9 and 48.1 MPa.

p0285 These values for shear stresses could be high or low depending on the magnitude of the stress normal to the fault. As described in Section 3, the effective stress normal to the fault ranged between 112 MPa (hydrostatic pore pressure) and 182 MPa (no pore pressure). Therefore, the ratio between shear stress and normal stress is in the range between 0.4 and 0.08, well below the friction coefficient typical for tonalites, and suggests fault lubrication by friction-induced melts.

s0075 5.2. Experimental Results

p0290 Fault lubrication by friction-induced melts is supported by nonconventional rock friction experiments performed with high-velocity rotary shear apparatuses on tonalite (described here) and other silicate-built rocks (gabbros, monzodiorites, peridotites; *Del Gaudio et al.*, 2006; *Hirose and Shimamoto*, 2005a). The effective slip velocities in these experiments (1 cm/s to 1.3 m/s for standard cylindrical samples with an external diameter of 22.3 mm) are comparable to slip rates achieved in earthquakes. Therefore, contrary to biaxial and triaxial apparatuses (total displacements <2 cm and slip rates <1 cm s^{-1}), it allows the investigation of the seismic slip. The apparatus has a horizontal arrangement, with a stationary shaft on one end and the rotating shaft on the opposite end. The stationary shaft provides up to 1 ton of axial thrust (corresponding to maximum normal stress of 20 MPa for a 22.3 mm in diameter solid sample) by means of a pneumatic axial load actuator. The rotary

shaft provides a rotary motion up to 25 rounds per second by means of an electric engine and an electromagnetic clutch (for a detailed description of the apparatus see *Hirose and Shimamoto*, 2005a; *Shimamoto and Tsutsumi*, 1994). Given the cylindrical shape of the samples, the determination of the slip rate and shear stress is problematic, because slip rate and torque (in the experiments are measured with the rotating speed and the torque) increase with sample radius r ($V = \omega r$; ω is the rotary speed). So the experimental data are obtained in terms of "equivalent slip rate" V_e (*Hirose and Shimamoto*, 2005a, 2005b; *Shimamoto and Tsutsumi*, 1994):

$$V_e = \frac{1}{\tau A}\int_{r_1}^{r_2} 4\pi^2\ \tau R r_i^2\ dr_i \tag{13}$$

p0295 where τ is the shear stress (assumed as constant over the sliding surface), A is the area of the sliding surface, R is the revolution rate of the motor, and r_1, r_2 are the inner and outer radius of a hollow cylindrical specimen, respectively. For solid cylindrical specimens, where $r_1 = 0$,

$$V_e = \frac{4\ \pi\ Rr}{3} \tag{14}$$

p0300 We refer to the equivalent slip rate simply as slip rate V hereafter.

p0305 In the experiments conducted on Adamello tonalite, slip rates were of $\sim 1\ \mathrm{m\,s^{-1}}$ and, when the normal stress was sufficiently high (i.e., 15 to 20 MPa), the total slip was a few meters at most, so comparable with deformation conditions typical of large earthquakes. Given the dramatic decrease in rock strength with increasing heat due to (1) thermal expansion of minerals and (2) the $\alpha - \beta$ transition in quartz, which by increasing the quartz volume by 5% renders the rock weak (thermal fracturing; *Ohtomo and Shimamoto*, 1994), higher normal stresses were achieved by using solid cylinders of rock confined with aluminum rings (Figures 7b and 7c). Because aluminum melts at 660°C, whereas most rock-forming minerals melt at more than 1000°C (*Spray*, 1992), the aluminum ring sustains the sample till bulk melting on the sliding surface occurs.

p0310 The experiments consisted of four main steps (1 to 4). In step 1, the axial thrust was applied to the sample. In step 2, the target rotation speed was achieved while an electromagnetic clutch split the rotating column from the specimen. In step 3, when the motor speed reached the target value, the electromagnetic clutch was switched on and the specimens started to slide. In step 4, the motor was switched off to end the experiment. The number of rotations, the axial force, the axial shortening of the specimen, and the torque were recorded by a digital recorder with a data sampling rate of 500 and 1000 Hz.

p0315 In the case of the Adamello tonalite, four experiments were conducted at constant slip rate ($1.28\ \mathrm{m\ s^{-1}}$) and increasing normal stress (5, 10, 15, and 20 MPa) (experiments with cataclasites yielded similar results; *Di Toro et al.*, 2006b). Similarly to the frictional melting model for the elastico-frictional crust

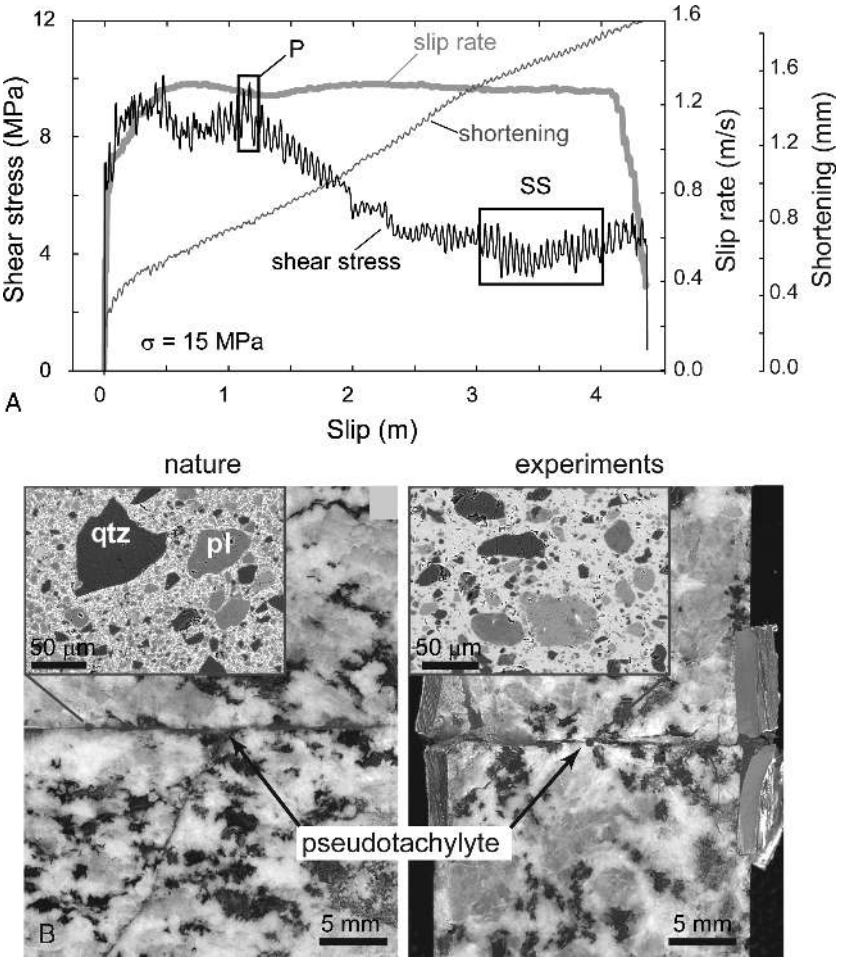

f0035 **FIGURE 7** Results and products of high-velocity rock friction experiments. (a) Shear stress, slip rate, and sample shortening versus slip curves for the Adamello tonalite. Boxes P and SS indicate the displacement intervals used to determine the peak and the steady-state shear stress, respectively, and are plotted in Figure 9a. (b) Comparison between natural (left) and artificial (right) pseudotachylyte. The insets are back-scatter electron scanning electron microscope images of the slipping zones. Both natural and artificial pseudotachylyte have quartz (qtz) and plagioclase (pl) clasts suspended in a cryptocrystalline (natural) and glassy (artificial) matrix. The cryptocrystalline matrix found in nature is explained by the higher ambient temperature in nature (~250°C) with respect to the lab (20°C) and the different cooling (and geological) history. All figures from *Di Toro et al.* (2006a).

(Figure 2b), production of melt in the experiments was preceded by production and extrusion of rock powder from the sample assembly. Melt was also extruded after the powder, similar to what is found in natural faults, where most of the melt is injected into the wall rock (e.g., Figure 4c). Extrusion resulted in a

progressive shortening of the sample with increasing slip. At the end of the experiments, a thin layer of melt (fault vein) separated the two opposite sliding surfaces. This artificial pseudotachylyte was remarkably similar to natural pseudotachylytes from the Gole Larghe Fault (Figures 7b and 7c).

p0320 In each experiment, the shear stress evolved with increasing slip: after an increase (strengthening stage) to a peak value (P in Figure 7a), shear stress decreased toward a steady-state value (SS in Figure 7a) through a transient stage whose length decreased with increasing normal stress. This evolution of shear stress with slip is typical of all the frictional melting experiments performed so far in different rocks (gabbro, peridotite, etc.; *Del Gaudio et al*., 2006; *Hirose and Shimamoto*, 2005a; *Tsutsumi and Shimamoto*, 1997a). The evolution of the shear stress with slip in these experiments can be correlated with the microstructural evolution of the melt layer (i.e., amount of clasts) and of the topography of the boundary between the melt and the wall rock (*Del Gaudio et al*., 2006; *Hirose and Shimamoto*, 2003, 2005a, 2005b). For instance, during the strengthening stage, the slipping zone is discontinuously decorated by melt patches, whereas, during the transient stage and the steady-state stage, the sliding surfaces are separated by a continuous layer of melt (*Del Gaudio et al*., 2006; *Hirose and Shimamoto*, 2005a, 2005b).

p0325 In each experiment with tonalite, the plot of peak and steady-state shear stress versus normal stress shows a slight dependence of shear stress with normal stress which can be roughly described by the equations:

$$\text{Peak shear stress} \quad \tau_p = 4.78 \text{ MPa} + 0.22\ \sigma \tag{15}$$

$$\text{Steady-state shear stress} \quad \tau_{ss} = 3.32 \text{ MPa} + 0.05\ \sigma \tag{16}$$

p0330 The "effective" friction coefficient, or ratio of shear stress versus normal stress, ranges between 0.05 and 0.22, which is well below Byerlee's friction (see Figure 8a). This suggests lubrication of the fault surfaces operated by frictional melts. By extrapolating the effective friction coefficient to seismogenic depth (i.e., to natural conditions where pseudotachylytes were found), experimental data fit well with the natural data (Figure 8b). Of course, the effective friction coefficient corresponds to the best fit line of the experimental data and does not describe the physics of the process. A better extrapolation, which considers the physics of the frictional melting and melt lubrication, is proposed in Section 5.3.

s0080 5.3. Theoretical Estimates

p0335 Theoretical derivations of the shear stress dependence on normal stress and slip rate in the presence of melt have been proposed (*Fialko and Khazan*, 2005; *Nielsen et al*., 2008). *Nielsen et al.* (2008) argued that a steady-state limit condition exists in case of melt extrusion, based on the balance of heat and mass flow during frictional melt. They derived an expression for shear resistance at the steady-state as a function of applied slip rate and normal

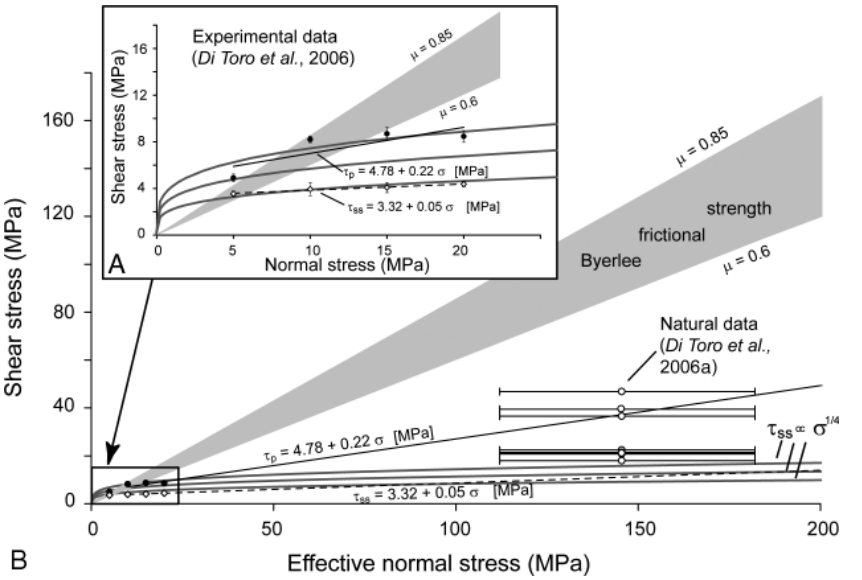

f0040 **FIGURE 8** Shear stress versus normal stress for experimental, natural, and theoretical data compared to solid friction for tonalite (modified from *Di Toro et al*., 2006a). (a) A zoombox showing the detail of experimental results. (b) The global representation including field estimates. The light gray area indicates the range of typical frictional values for tonalite (*Byerlee*, 1978). Solid circles and open diamonds are experimental values for peak shear stress and steady-state shear stress (Figure 7). Field data have a large range of effective normal stress (as indicated by the length of the horizontal error bar) due to the poorly constrained pore pressure at the time of seismic faulting during the Gole Larghe earthquakes. The solid line is the best linear fit for the peak shear stress data (Equation 15); the dashed line is the best linear fit line for the steady-state shear stress (Equation 16). The three gray curves represent theoretical predictions for viscous strength assuming $\tau_{ss} = \alpha\, \sigma^{0.25}$ (according to Equation 22) and setting $\alpha = 8 \times 10^4$, 11×10^4, and 14×10^4, respectively.

stress. In their model, melt thickness, temperature, and viscosity profile are not imposed but result from the coupling of viscous shear heating, thermal diffusion, and melt extrusion. In fact, lubrication does not automatically arise from the simple presence of melt; indeed a thin layer of high-viscosity melt may induce strengthening of the interface (*Koizumi et al*., 2004; *Scholz*, 2002). Thus, the determination and combination of melt temperature, composition and clast content (which all affect melt viscosity), and melt layer thickness are needed to estimate shear resistance. These parameters themselves depend on the extrusion rate (squeezing of melt under normal stress tending to reduce the thickness of the layer), melting rate (providing new melt tending to increase the layer thickness), and strain rate in the melt layer (affecting heat production, hence altering melting rate, melt temperature, and melt viscosity). In other words, lubrication is the result of a complex feedback between viscosity, normal stress, and slip rate as quantified in *Nielsen et al*. (2008).

p0340 The existence of a steady-state is also manifest in the experimental results, which indicate that melt thickness (*Hirose and Shimamoto*, 2005a) and shortening rate tend to a stable value after a variable amount of slip (Figure 7a). From simple mass conservation arguments, constant thickness and shortening rate imply that melting and extrusion rates are constant too. Heat is produced by the viscous shear of the melt layer and removed through (1) extrusion of hot melt, (2) latent heat for melting, and (3) diffusion into the wall rocks. However, because the rock is consumed by the advancement of melting (shortening), the advancement of heat by diffusion into the rock is compensated by the shortening rate. As a consequence, the isotherms are fixed in space and time with respect to the sliding interface; a solid particle belonging to the rock sample moves toward the interface and traverses the isotherms until it melts, and, finally, it is extruded from the sample assembly (Figure 9a). The complex physics of frictional melt lubrication is described by a system of five differential equations (*Nielsen et al*., 2008), which describe the following:

o0030 **1.** *Melting at the solid interface* (the Stefan problem, *Turcotte and Schubert*, 2002):

$$\rho\ L\ v = \kappa\ \rho\ c_p \left.\frac{\partial T}{\partial z}\right|_{w+} - \kappa_m \rho_m c_{pm} \left.\frac{\partial T}{\partial z}\right|_{w-} \tag{17}$$

where $L = H\,(1\text{-}\phi)$ is effective latent heat, v is shortening rate, κ, ρ, c are the thermal diffusivity, mass density, and heat capacity of the solid

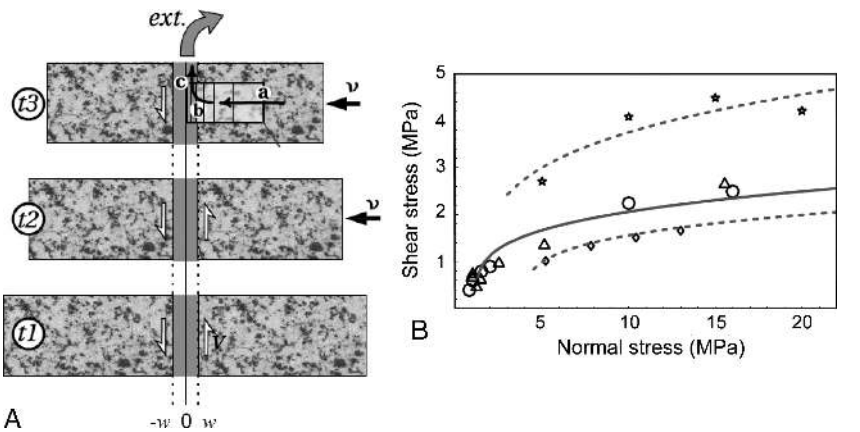

f0045 **FIGURE 9** Estimate of dynamic fault strength: the theoretical model. (a) A cartoon explaining the geometry of the shear/shortening mechanism analyzed, inside a rock volume, at three successive time steps *t1, t2*, and *t3*. The central gray area represents the melt layer of half-thickness *w*. The white arrows represent the shear motion, whereas the lateral arrows represent the convergent motion of the blocks due to the shortening process. (b) Fitting of experimental data according to Equation 22 for peridotite (diamonds), gabbro, monzodiorite (triangles and circles, respectively), and tonalite (stars). Reproduced with permission from *Nielsen et al*. (2008).

B978-0-12-374452-4.00005-2, 00005

(whereas melt parameters are denoted by the subscript m), and the two derivatives at w^- and w^+ represent temperature gradient on the melt side and on the solid side, respectively;

o0035 **2.** *Heat diffusion at the steady-state*, with a mass flow at velocity ν and a heat source density due to shear rate $\dot{\epsilon}$ (the equation is slightly simplified in either the solid or the melt: heat source is zero inside the solid, whereas it can be shown that heat transfer by flow is negligible inside the melt):

$$\kappa_m \frac{\partial^2 T}{\partial z^2} + \frac{\tau_{ss}\dot{\varepsilon}}{\rho_m c_m} - v\frac{\partial T}{\partial z} = 0 \tag{18}$$

o0040 **3.** *The normal stress σ_n supported by a layer of melt* of equivalent viscosity η_e being squeezed at a rate (which corresponds to the shortening rate of the specimen) v:

$$\sigma_n = C\frac{\eta_e v L_e^2}{w^3} \tag{19}$$

with C a geometrical factor ($C = 3/16$ for a solid cylinder), w the melt layer half thickness and L_e the escaping distance of the frictional melt from the sliding surface (in experiments, L_e is about the radius of the sample: in nature, L_e is the half distance between injection veins, e.g., decimeters to meters).

o0045 **4.** *The strain rate* within the melt layer of thickness z and viscosity η:

$$\dot{\varepsilon}(z) = \frac{\tau_{ss}}{\eta(z)} \tag{20}$$

o0050 **5.** *The viscosity dependence on temperature T* (note that the viscosity law adopted is rather simplified: it is a linearization of the exponential law for a Newtonian fluid):

$$\eta(T) = \eta_c \exp(-(T - T_m)/T_c) \tag{21}$$

where $T_c = {T_m}^2/B$ and $\eta_c = A\exp(B/T_m)$ are the characteristic temperature and viscosity of the melt of temperature T_m. Values of η_c and T_c may be estimated based on composition, clast content, and a well-known empirical viscosity law (*Shaw*, 1972; *Spray*, 1993). Note that this only leads to a very rough estimate, given that the result is highly dependent on clast concentration and melt composition; furthermore, it assumes that the melt behaves as a Newtonian fluid (viscosity independent of shear rate), which is probably not the case here. As a consequence, *a priori* estimates of η_c, T_c are only indicative for the time being and shall require a substantial analysis of experimental and natural samples, which has started.

p0385 The coupled of the preceding system of differential equations may be solved analytically, yielding an expression for shear stress in closed form (*Nielsen et al.*, 2008):

B978-0-12-374452-4.00005-2, 00005

$$\tau_{ss} = \sigma^{0.25} \frac{N_f}{\sqrt{L_e}} \sqrt{\frac{\log(2V/W)}{V/W}} \tag{22}$$

p0390 where N_f is a normalizing factor, L_e is function of the geometry of the sample (it is related to the escaping distance of the frictional melt from the sliding surface), V is slip rate, and W is a factor with velocity dimensions, grouping six constitutive parameters:

$$W = \sqrt{\frac{8T_c\kappa_m\rho_m c_{pm}}{\eta_c}} \tag{23}$$

p0395 The corresponding melt half-thickness is also obtained as

$$w = \frac{W\eta_c}{\tau_{ss}} \frac{\operatorname{arctanh}\left(\frac{\frac{V}{W}}{\sqrt{\left(\frac{V^2}{W^2}+1\right)}}\right)}{\sqrt{\left(\frac{V^2}{W^2}+1\right)}} \tag{24}$$

p0400 Finally, details of the inhomogeneous viscosity and temperature profiles across the melt layer may be found in *Nielsen et al*. (2008). Note that Equation 19 assumes that all of the normal load is supported by viscous push of the melt layer. A more complex normal stress dependence could arise if hydrodynamic push, bubble formation, or interaction at the asperity contacts or through clast clusters play an important role. In spite of the simplifying assumptions, the shear stress curves obtained are in reasonable agreement with the experimental data. Specific experiments on gabbro tested the relationship between steady-state shear stress and, for instance, normal stress while the other variables (e.g., slip rate V) were kept constant (e.g., Figure 8b).

p0405 To extrapolate Equation 22 to the ambient conditions of the Gole Larghe paleoearthquakes, we used $\tau_{ss} = \alpha\, \sigma^{0.25}$ (by grouping all parameters other than stress into a single value α) and set $\alpha = 8 \times 10^4$. The equation fits reasonably well both the experimental data and the field estimates, corroborating the idea of effective lubrication in the presence of friction melts (Figure 9b); curves obtained for alternative values of $\alpha = 11 \times 10^4$ and 14×10^4 are also represented.

s0085 6. DISCUSSIONS AND CONCLUSIONS

p0410 The study of the Adamello Faults and associated pseudotachylytes has the potential to unravel aspects of rupture dynamics and fault strength during seismic slip. The "direct" investigation of the exhumed seismic fault network in the Adamello, following the pioneering work of *Sibson* (1975) on pseudotachylytes, has proven an outstanding source of information, complementary to seismological information, if integrated with calibrated experimental and

B978-0-12-374452-4.00005-2, 00005

theoretical analysis. This approach deserves future efforts and extension to this and other natural laboratories.

p0415 Field description of natural pseudotachylyte-bearing faults as well as theoretical models and physical experiments all need improvements to better describe the process of seismic faulting. Field description needs detailed quantitative methods to map the 3D geometry of the fault zone and the pseudotachylyte distribution between and along the different fault segments. Also, there is the need to further investigate how the results of experimental and theoretical studies, performed under simplified conditions and geometries, can be extrapolated to earthquake source mechanics. For instance, the constitutive equation for frictional melt lubrication (Equation 22), though tested in the laboratory, describes the shear stress during steady-state conditions of slip; however, abrupt variations in slip rate and normal stress (the so-called transient stage) occur in nature (e.g., *Beeler and Tullis*, 1996). In addition, current experiments and theoretical models do not take into account the geometry and complexity of natural faults. The presence of bumps on a fault surface (*Power et al*., 1988; *Sagy et al*., 2007) might impede the smooth sliding reproduced in the laboratory, and future studies should consider the effects of fault roughness on frictional sliding. Though this is difficult to investigate in experiments due to the small size of the samples and technical limitations, the problem can be tackled by numerical models, which include the fault roughness and the constitutive law (including the transient stage) for melt lubrication. The input roughness of the fault for the numerical model can be imported directly from quantitative field reconstruction of the fault geometry (e.g., by light detection and ranging [LIDAR]; see also Section 6.1).

p0420 The dependence of shear stress with slip rate in the presence of friction melts may have dramatic effects on the rupture propagation process. The outcome of the abrupt decrease in slip rate on the shear stress is shown in an experiment performed at low normal stress (0.72 MPa) on hollow-shaped (24.9 mm and 15.6 mm external and internal diameter, respectively) gabbro samples (Figure 10) (*Di Toro and Hirose*, unpublished data). Once the steady-state shear stress was achieved, the perturbation induced in the system "melt layer plus apparatus" by decreasing the slip rate from 1.6 to 0.8 m s^{-1} resulted in an abrupt increase in strength and the achievement of an unstable regime (see the stick-slip–like behavior after about 115 m of slip). Such abrupt increase in strength may produce self-healing rupture pulses in nature and may result in lower stress drops than those retrieved from the current theoretical models and experimental data.

p0425 A main result of the integrated studies shown in this contribution is the recognition of fault lubrication by frictional melts during earthquakes. An expected outcome of melt lubrication is the occurrence of large dynamic stress drops, especially at depth. Field, experimental, and theoretical data summarized in Figure 9 all indicate stress drops in the range of 40 to 120 MPa at 10 km depth. However, these stress drops are larger than those

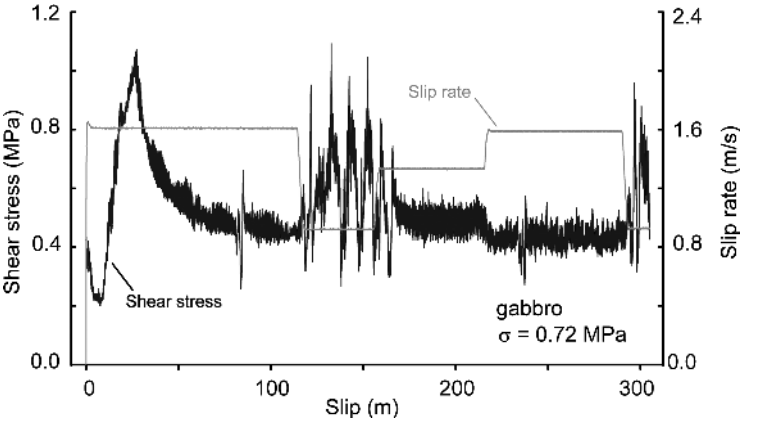

f0050 **FIGURE 10** Dependence of shear stress with slip rate in the presence of frictional melts. For a particular combination of slip rate and normal stress (in this case, $V = 0.8$ m/s and $\sigma = 0.72$ MPa), the shear stress is highly unstable (see the seven peaks of high shear stress between 115 and 170 m of slip). Though poorly investigated, the nonlinear dependence of shear stress with slip rate may explain rupture heal and self-healing pulses. The large displacement achieved in this experiment is the result of the application of a small normal stress (compare with Figure 7a).

expected in the upper crust from seismological investigations (between 0.1 and 30 MPa according to *Hanks*, 1977). This discrepancy well illustrates the uncertainties of extrapolating our results to nature and to match our observation with seismological data. The reasons for the "stress drop" discrepancy can be multifold, including the fact that the actual experimental and theoretical models might fail to completely describe the seismic slip process (as underlined earlier). But a reasonable explanation for the discrepancy could be that we estimated *dynamic* stress drops, whereas those considered by *Hank*s (1977) were *static* stress drops (e.g., *Scholz*, 2002, p. 204). *Bouchon* (1997) estimated dynamic stress drop as large as 100 MPa in several discrete fault elements (mostly located at about 10 km depth, so at ambient conditions similar to those in the Gole Larghe Fault zone) during the Loma Pietra M_L 6.9, 1989 earthquake. Another possible explanation for the lower stress drops retrieved by seismology is that frictional melting is rare in nature and that the stress drops we estimated occur only in some special cases. According to *Sibson and Toy* (2006), pseudotachylytes are not common between fault rocks and, therefore, other coseismic weakening mechanisms (e.g., thermal pressurization, flash heating; *Bizzarri and Cocco*, 2006; *Rice*, 2006) may be more relevant than melt lubrication. We believe, however, that frictional melting is common in silicate-built rocks during faulting in the lower part of the brittle crust as supported, for example, by the widespread occurrence of pseudotachylytes reported in the European Alps. A reason for the apparent scarcity of pseudotachylyte is probably due to the elusive nature of these fault rocks

B978-0-12-374452-4.00005-2, 00005

(e.g., veins are thin and pristine "magmatic" structures may easily undergo alteration during postseismic deformation and fault exhumation; for a detailed discussion, see *Di Toro et al*., 2006b). It follows that pseudotachylytes can be easily missed in the field, even in locales investigated, in detail, for decades (see the case for the pseudotachylyte recently found in the Mount Abbot quadrangle in Sierra Nevada, California; *Griffith et al*., 2008; *Kirkpatrick et al*., 2007). In any case, it is worth noting that all friction experiments performed so far on cohesive and noncohesive rocks at seismic slip rates indicate the activation of some weakening mechanisms (thermal decomposition, gouge-related weakening, silica gel lubrication) that, in the absence of frictional melts, produce a dramatic decrease in shear stress similar to that observed in the case of melt lubrication (*Di Toro and Nielsen*, 2007; *Wibberley et al.,* 2008). The discrepancy between experimental results and seismological observations suggests that other factors including the dependence of the shear stress with slip rate and the roughness of the fault surface should be considered in rupture dynamics models in order to extrapolate experimental observations to natural conditions.

s0090

6.1. A New Approach to the Study of Exhumed Pseudotachylyte-Bearing Faults

p0430

The review of previous work shows that it is possible to retrieve information on earthquake mechanics from pseudotachylyte-bearing fault-fracture networks. However, a realistic physical model of the earthquake source should include, for instance, the roughness of natural fault surfaces, because fault geometry controls nucleation, propagation, and arrest of the seismic rupture (e.g., asperity and barriers; *Scholz*, 2002).

p0435

The synoptic view of Figure 11 summarizes an ideal multidisciplinary approach for the study of the earthquake mechanics by "direct" investigation of exhumed faults. The 3D architecture of an exhumed seismogenic fault zone is the basic input parameter for modeling coseismic fault slip and rupture propagation and requires a complete 3D mapping of fault geometry and distribution of different fault rocks within and between the different elements of the deformation network. To this aim, classical field structural analysis can be integrated with high-resolution laser scan (light detection and ranging [LIDAR]) mapping, allowing the reconstruction of fault zone architecture with a millimeter scale precision over large outcrops in the case of the Adamello Fault zone (Figure 11a). LIDAR and conventional structural data can be processed by geomodeling platforms to produce "true" 3D models of fault zones (*Jones et al*., 2004) (Figure 11b). A further step to understanding earthquake processes from the field studies of exhumed fault zones will be the upscaling of analysis from the outcrop (10^2 to 10^3 m) to the large earthquake scale (10^4 to 10^5 m). This can be accomplished using geostatistical techniques developed in the oil industry (*Mallet*, 2002). The mapped 3D geometries of the fault zone will form the reference of calibrated numerical

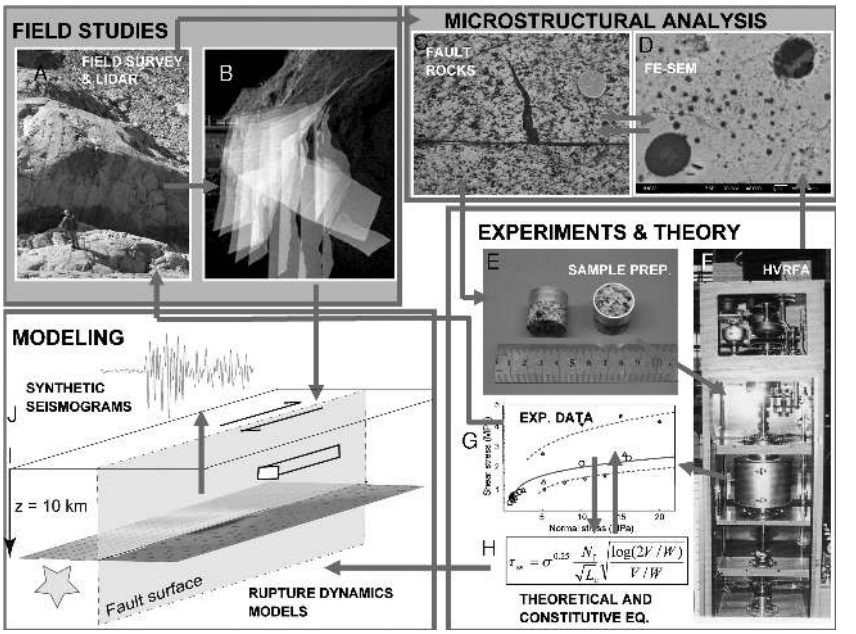

f0055 **FIGURE 11** A multidisciplinary approach to the study of pseudotachylyte-bearing fault networks: synoptic view (see the text for an explanation). The BSE-SEM image in Figure 11d is courtesy of INGV. **(See Color Plate 15.)**

simulations for rupture nucleation and propagation (Figure 11i) (see Section 4). On a parallel line of research, samples from the fault zone (Figure 11c) are prepared (Figure 11e) and tested in rock friction experiments (Figure 11f) to investigate their frictional behavior during the seismic cycle (Figure 11g) (Section 5.2). Natural and experimentally produced fault rocks are analyzed in the lab (through microstructural, geochemical, and mineralogical analysis (Figure 11d) and compared to determine deformation processes. Constitutive and theoretically based equations (Figure 11h) that describe the rheology of the fault materials are tested in the nonconventional rock friction apparatus (Figures 11e, 11f, and 11g) (see Section 5.3). The experimental results (e.g., magnitude of the fault shear strength during seismic slip) are also checked in the field (Figures 11a and 11g) (see Section 5.1). The fault rheology constitutive equations (Figure 11h) are then applied in rupture models (Figure 11i) of real faults (Figures 11a and 11b). Earthquake rupture modeling (Figure 11i) will generate synthetic seismograms (Figure 11j) (*Olsen et al.*, 1997) to compare to real seismograms.

p0440 The multidisciplinary approach suggested here may exploit the extraordinary wealth of information frozen in large exposures of pseudotachylyte-bearing fault networks and yields a new vision of earthquake mechanics based on the physical processes occurring at seismogenic depth.

B978-0-12-374452-4.00005-2, 00005

ACKNOWLEDGMENTS

p0445 The authors thank Eiichi Fukuyama for editorial work, and we thank Hideo Takagi and an anonymous reviewer for their detailed and accurate comments to the paper. GDT and SN thank Takehiro Hirose and Toshihiko Shimamoto for allowing, helping, and running rock friction experiments at Kyoto University. This research was funded by the Fondazione Cariparo (Progetti di Eccellenza 2006), the University of Padova Scientifica fondi quota ex 60%, the European Research Council Starting Grant Project USEMS (2008–2013), and MIUR (PRIN2005). GDT thanks Elena Narduzzo for field support.

REFERENCES

Allen, A. R., (1979), Mechanism of frictional fusion in fault zones, *J. Struct. Geol.*, **1**, 231-243.

Allen, J. L., (2005), A multi-kilometer pseudotachylyte system as an exhumed record of earthquake rupture geometry at hypocentral depths (Colorado, USA), *Tectonophys.*, **402**, 37-54.

Andrews, J. D., (2005), Rupture dynamics with energy loss outside the slip zone, *J. Geophys. Res.*, **110**, B01307, doi:10.1029/2004JB003191.

Archard, J. F., (1958), The temperature of rubbing surfaces, *Wear*, **2**, 438-455.

Austrheim, H. and T. M. Boundy, (1994), Pseudotachylytes generated during seismic faulting and eclogitization of the deep crust, *Science*, **265**, 82-83.

Beeler, N. M. and T. E. Tullis, (1996), Self-healing slip pulses in dynamic rupture models due to velocity dependent strength, *Bull. Seismol. Soc. Am.*, **86**(4), 1130-1148.

Beeler, N. M., (2006), Inferring earthquake source properties from laboratory observations and the scope of lab contributions to source physics, In: *Earthquakes: Radiated Energy and the Physics of Faulting*, edited by Abercrombie, R., A. McGarr., G. Di Toro, and H. Kanamori, *Geophysical Monograph Series*, **170**, 99-119, American Geophysical Union, Washington, D.C.

Blenkinsop, T. G., (2000), *Deformation Microstructures and Mechanisms in Minerals and Rocks*, Kluwer Academic Publishers, pp. 1-132.

Bizzarri, A. and M. Cocco, (2006), A thermal pressurization model for the spontaneous dynamic rupture propagation on a three-dimensional fault: 1. Methodological approach, *J. Geophys. Res.*, **111**, B05303, doi:10.1029/2005JB003862.

Bossière, G., (1991), Petrology of pseudotachylytes from the Alpine Fault of New Zealand, *Tectonophys.*, **196**, 173-193.

Bouchon, M., (1997), The state of stress on same faults of the San Andreas system as inferred from near-field strong motion data, *J. Geophys. Res.*, **102**(B6), 11731-11744.

Bouchon, M. and M. Vallée, (2003), Observation of long supershear rupture during the magnitude 8.1 Kunlunshan earthquake, *Science*, **301**, 824-826.

Boullier, A.-M., T. Ohtani, K. Fujimoto, H. Ito, and M. Dubois, (2001), Fluid inclusions in pseudotachylytes from the Nojima fault, Japan, *J. Geophys. Res.*, **106**(B10), 21965-21977.

Brodsky, E. E. and H. Kanamori, (2001), Elastohydrodynamic lubrication of faults, *J. Geophys. Res.*, **106**(B8), 16357-16374.

Brune, J. N., S. Brown, and P. A. Johnson, (1993), Rupture mechanism and interface separation in foam rubber models of earthquakes: A possible solution to the heat flow paradox and the paradox of large overthrusts, *Tectonophys.*, **218**(1-3), 59-67.

Burridge, R., G. Conn, and L. B. Freund, (1979), The stability of a rapid mode II shear crack with finite cohesive traction, *J. Geophys. Res.*, **85**, 2210-2222.

Byerlee, J. D., (1978), Friction of rocks, *Pure Appl. Geophys.*, **116**, 615-626.

Camacho, A., R. H. Vernon, and J. D. Fitz Gerald, (1995), Large volumes of anhydrous pseudotachylyte in the Woodroffe Thrust, eastern Musgrave Ranges, Australia, *J. Struct. Geol.*, **17**, 371-383.

Callegari, E. and P. Brack, (2002), Geological map of the Tertiary Adamello batholith (Northern Italy)—Explanatory notes and legend, *Mem. Sci. Geol.*, **54**, 19-49.

Chambon, G., J. Schmittbuhl, and A. Corfdir, (2002), Laboratory gouge friction: Seismic-like slip weakening and secondary rate- and state-effects, *Geophys. Res. Lett.*, **29**(10), 1366, doi:10.1029/2001GL014467.

Chester, F. M., J. P. Evans, and R. L. Biegel, (1993), Internal structure and weakening mechanisms of the San Andreas fault, *J. Geophys. Res.*, **98**(B1), 771-786.

Clarke, G. L. and A. R. Norman, (1993), Generation of pseudotachylite under granulite facies conditions, and its preservation during cooling, *J. Metam. Geol.*, **11**, 319-335.

Cowan, D. S., (1999), Do faults preserve a record of seismic slip? A field geologist's opinion, *J. Struct. Geol.*, **21**(8-9), 995-1001.

Del Gaudio, P., R. Han, G. Di Toro, T. Hirose, T. Shimamoto, and M. Cocco, (2006), Dynamic strength of peridotite at seismic slip rates: Experimental results. *EOS, Trans., AGU*, **87**(52), Fall Meeting Suppl. Abst., S33A-0219.

Del Moro, A., G. Pardini, C. Quercioli, I. Villa, and E. Callegari, (1983), Rb/Sr and K/Ar chronology of Adamello granitoids, Southern Alp, *Mem. Soc. Geol. Ital.*, **26**, 285-299.

Dieterich, J. H., (1978), Time-dependent friction and the mechanics of stick-slip, *Pure Appl. Geophys.*, **116**(4-5), 790-806.

Dieterich, J. H., (1979), Modeling of rock friction 1. Experimental results and constitutive equations, *J. Geophys. Res.*, **84**, 2161-2168.

Di Toro, G. and G. Pennacchioni, (2004), Superheated friction-induced melts in zoned pseudotachylytes within the Adamello tonalites (Italian Southern Alps), *J. Struct. Geol.*, **26**, 1783-1801.

Di Toro, G. and G. Pennacchioni, (2005), Fault plane processes and mesoscopic structure of a strong-type seismogenic fault in tonalites (Adamello batholith, Southern Alps), *Tectonophys.*, **402**, 54-79.

Di Toro, G., D. L. Goldsby, and T. E. Tullis, (2004), Friction falls towards zero in quartz rock as slip velocity approaches seismic rates, *Nature*, **427**, 436-439.

Di Toro, G., S. Nielsen, and G. Pennacchioni, (2005a), Earthquake rupture dynamics frozen in exhumed ancient faults, *Nature*, **436**, 1009-1012.

Di Toro, G., G. Pennacchioni, and G. Teza, (2005b), Can pseudotachylytes be used to infer earthquake source parameters? An example of limitations in the study of exhumed faults, *Tectonophys.*, **402**, 3-20.

Di Toro, G., T. Hirose, S. Nielsen, G. Pennacchioni, and T. Shimamoto, (2006a), Natural and experimental evidence of melt lubrication of faults during earthquakes, *Science*, **311**, 647-649.

Di Toro, G., T. Hirose, S. Nielsen, and T. Shimamoto, (2006b), Relating high-velocity rock friction experiments to coseismic slip in the presence of melts, In: *Earthquakes: Radiated Energy and the Physics of Faulting*, edited by Abercrombie, R., A. McGarr, G. Di Toro, and H. Kanamori, *Geophysical Monograph Series*, **170**, 121-134, American Geophysical Union, Washington, D.C.

Di Toro, G., and S. Nielsen, (2007), Low dynamic fault strength at seismic slip rates: Experimental evidence, *XXIV General Assembly of the International Union of Geodesy and Geophysics*, abstract SW 003.

B978-0-12-374452-4.00005-2, 00005

Ermanovics, I. F., H. Helmstaedt, and A. G. Plant, (1972), An occurrence of Archean pseudotachylite from Southern Manitoba, *Can. J. Earth Sci*, **9**, 257-265.

Fabbri, O., A. Lin, and H. Tokushige, (2000), Coeval formation of cataclasite and pseudotachylyte in a Miocene forearc granodiorite, southern Kyushu, Japan, *J. Struct. Geol.*, **22**, 1015-1025.

Fialko, Y., (2004), Temperature fields generated by the elastodynamic propagation of shear cracks in the Earth, *J. Geophys. Res.*, **109**, B01303, doi:10.1029/2003JB002497.

Fialko, Y. and Y. Khazan, (2005), Fusion by earthquake fault friction: Stick or slip?, *J. Geophys. Res.*, **110**, B12407, doi:org/10.1029/2005JB003869.

Francis, P. W., (1972), The pseudotachylyte problem, comments on earth sciences, *Geophys.*, **3**, 35-53.

Goldsby, D. L. and T. E. Tullis, (2002), Low frictional strength of quartz rocks at subseismic slip rates, *Geophys. Res. Lett.*, **29**(17), 1844, doi:10.1029/2002GL01240.

Griffith, W. A., G. Di Toro, G. Pennacchioni, and D. D. Pollard, (2008), Thin pseudotachylytes in faults of the Mt. Abbot Quadrangle, Sierra Nevada: Physical constraints for small seismic slip events. *J. Struct. Geol.*, **30**, 1086-1094.

Griffith, W.A., A.J. Rosakis, D.D. Pollard and C. Ko, (2008), Tensile cracks: a new link between geological observations of faults and seismological models of earthquake dynamics, *American Geophysical Union, Eos Trans.* **89**(53), abstract T22A-05.

Grocott, J., (1981), Fracture geometry of pseudotachylyte generation zones: A study of shear fractures formed during seismic events, *J. Struct. Geol.*, **3**, 169-178.

Grunewald, U., R. S. J. Sparks, S. Kearns, and J. C. Komorowski, (2000), Friction marks on blocks from pyroclastic flows at the Soufriere Hills volcano, Montserrat: Implication for flow mechanisms, *Geology*, **28**, 827-830.

Guatteri, M. and P. Spudich, (1998), Coseismic temporal changes of slip direction; the effect of absolute stress on dynamic rupture, *Bull. Seismol. Soc. Am.*, **88**, 777-789.

Guatteri, M. and P. Spudich, (2000), What can strong-motion data tell us about slip-weakening fault-friction laws?, *Bull. Seismol. Soc. Am.*, **90**, 98-116.

Han, R., T. Shimamoto, T. Hirose, J.-H. Ree, and J. Ando, (2007), Ultralow friction of carbonate faults caused by thermal decomposition, *Science*, **316**, 878-881.

Hanks, T. C., (1977), Earthquake stress drops, ambient tectonic stresses and stresses that drive plate motions, *Pure Appl. Geophys.*, **143**, 441-458.

Heaton, T. H., (1990), Evidence for and implications of self healing pulses of slip in earthquake rupture, *Phys. Earth Planet. Interi.*, **64**, 1-20.

Hickman, S., M. Zoback, and W. Ellsworth, (2004), Introduction to special section: Preparing for the San Andreas Fault Observatory at Depth, *Geophys. Res. Lett.*, **31**, L12S01, doi:10.1029/2004GL020688.

Hirose, T. and T. Shimamoto, (2003), Fractal dimension of molten surfaces as a possible parameter to infer the slip-weakening distance of faults from natural pseudotachylytes, *J. Struct. Geol.*, **25**, 1569-1574.

Hirose, T. and T. Shimamoto, (2005a), Growth of molten zone as a mechanism of slip weakening of simulated faults in gabbro during frictional melting, *J. Geophys. Res.*, **110**, B05202, doi:10.1029/2004JB003207.

Hirose, T. and T. Shimamoto, (2005b), Slip-weakening distance of faults during frictional melting as inferred from experimental and natural pseudotachylytes, *Bull. Seismol. Soc. Am.*, **95**, 1666-1673.

Holland, T. H., (1900), The charnokite series, a group of Archean hypersthenic rocks in peninsular India, *India Geological Survey Memories*, **28**, 119-249.

Ida, Y., (1972), Cohesive force across the tip of a longitudinal shear crack and Griffith's specific surface energy, *J Geophys. Res*., **77**, 3796-3805.

Irwin, G. R., (1957), Analysis of stresses and strains near the end of a crack traversing a plate, *J. Appl. Mech*., **24**, 361-364.

Jeffreys, H., (1942), On the mechanics of faulting, *Geol. Mag*., **79**, 291-295.

Jones, R. R., K. J. W. McCaffrey, R. W. Wilson, and R. E. Holdsworth, (2004), Digital field data acquisition: Towards increased quantification of uncertainty during geological mapping, In: *Geological Prior Information*, edited by Curtis, A., and R. Wood, *Geological Society Special Publication*, **239**, 43-56.

Kanamori, H., D. L. Anderson, and T. H. Heaton, (1998), Frictional melting during the rupture of the 1994 Bolivian earthquake, *Science*, **279**, 839-842.

Kanamori, H. and E. Brodsky, (2004), The physics of earthquakes, *Rep. Prog. Phys*., **67**, 1429-1496.

Kirkpatrick, J. D., Z. K. Shipton, J. P. Evans, S. Micklethwaite, S. J. Lim, and P. McKillop (2008), Strike-slip fault terminations at seismogenic depths: The structure and kinematics of the Glacier Lakes fault, Sierra Nevada United States, *J. Geophys. Res*., **113**, B04304, doi:10.1029/2007JB005311.

Koizumi, Y., K. Otsuki, A. Takeuchi, and H. Nagahama, (2004), Frictional melting can terminate seismic slips: Experimental results of stick-slip, *Geophys. Res. Lett*., **31**, L21605, doi:10.1029/2004GL020642.

Kostrov, B., (1964), Self-similar problems of propagation of shear cracks, *J. Appl. Mech*., **28**, 1077-1087.

Kostrov, B. and S. Das, (1988), *Principles of Earthquake Source Mechanics*, Cambridge Univ. Press, London.

Lachenbruch, A. H., (1980), Frictional heating, fluid pressure, and the resistance to fault motion, *J. Geophys. Res*., **85**(B11), 6249-6272.

Lee, W. H., H. Kanamori, P. C. Jennings, and C. Kisslinger, (2002), *International Handbook of Earthquake & Engineering Seismology*, Part A & B, Academic Press, Amsterdam.

Lin, A., (1994), Glassy pseudotachylytes from the Fuyun Fault Zone, Northwest China, *J. Struct. Geol*., **16**, 71-83.

Lin, A. and T. Shimamoto, (1998), Selective melting processes as inferred from experimentally generated pseudotachylytes, *J. Asian Earth Sci*., **16**, 533-545.

Lin, A., A. Chen, C. Liau, C. Lee, C. Lin, P. Lin, S. Wen, and T. Ouchi, (2001), Frictional fusion due to coseismic slip landsliding during the 1999 Chi-Chi (Taiwan) ML 7.3 earthquake, *Geophys. Res. Lett*., **28**, 4011-4014.

Lin, A., (2007), *Fossil Earthquakes: The Formation and Preservation of Pseudotachylytes*, Springer, Berlin, 348 pp.

Lockner, D. A. and N. M. Beeler, (2002), Rock failure and earthquakes, In: *Earthquake & Engineering Seismology*, edited by Lee, W. H., H. Kanamori, P. C. Jennings, and C. Kisslinger, 505-537, Academic Press, Amsterdam.

Lockner, D. A. and P. G. Okubo, (1983), Measurements of frictional heating in granite, *J. Geophys. Res*., **88**, 4313-4320.

Ma, K.-F., S.-R. Song, H. Tanaka, C.-Y. Wang, J.-H. Hung, Y.-B. Tsai, J. Mori, Y.-F. Song, E.-C. Yeh, H. Sone, L.-W. Kuo, and H.-Y. Wu, (2006), Slip zone and energetics of a large earthquake from the Taiwan Chelungpu-fault Drilling Project (TCDP), *Nature*, **444**, 473-476.

Maddock, R. H., (1983), Melt origin of fault-generated pseudotachylytes demonstrated by textures, *Geology*, **11**, 105-108.

B978-0-12-374452-4.00005-2, 00005

Maddock, R. H., (1986), Partial melting of lithic porphyroclasts in fault-generated pseudotachylytes, *Neues Jahrbuch für Mineralogie—Abhandlungenr*, **155**, 1-14.

Maddock, R. H., J. Grocott, and M. Van Nes, (1987), Vesicles, amygdales and similar structures in fault-generated pseudotachylytes, *Lithos*, **20**, 419-432.

Maddock, R. H., (1992), Effects of lithology, cataclasis and melting on the composition of fault-generated pseudotachylytes in Lewisian gneiss, Scotland, *Tectonophys*., **204**, 261-278.

Magloughlin, J. F., (1989), The nature and significance of pseudotachylite from the Nason terrane, North Cascade Mountains, Washington, *J. Struct. Geol*., **11**, 907-917.

Magloughlin, J. F., (1992), Microstructural and chemical changes associated with cataclasis and frictional melting at shallow crustal levels: The cataclasite-pseudotachylyte connection, *Tectonophys*., **204**, 243-260.

Magloughlin, J. F. and J. G. Spray, (1992), Frictional melting processes and products in geological materials: Introduction and discussion, *Tectonophys*., **204**, 197-206.

Magloughlin, J. F., (2005), Immiscible sulfide droplets in pseudotachylyte: Evidence for high temperature ($>1200^{\circ}C$) melts, *Tectonophys*., **402**, 81-91.

Mallet, J. L., (2002), *Geomodelling*, Oxford Univ. Press, Oxford.

Marone, C., (1998), Laboratory-derived friction laws and their application to seismic faulting, *Ann. Rev. Earth Planet. Sci*., **26**, 643-696.

Masch, L., R. H. Wenk, and E. Preuss, (1985), Electron microscopy study of hyalomylonites—Evidence for frictional melting in landslides, *Tectonophys*., **115**, 131-160.

Mase, C. W. and L. Smith, (1987), Effects of frictional heating on the thermal, hydrologic, and mechanical response of a fault, *J. Geophys. Res*., **92**(B7), 6249-6272.

Mayeda, K. and W. R. Walter, (1996), Moment, energy, stress drop, and source spectra of western United States earthquakes from regional coda envelopes, *J. Geophys. Res*., **101**, 11, 195-11208.

McKenzie, D. and J. N. Brune, (1972), Melting on fault planes during large earthquakes, *Geophys. J. Roy. Astr. Soc*., **29**, 65-78.

McPhie, J., M. Doyle, and R. Allen, (1993), *Volcanic Textures: A Guide to the Interpretation of Textures in Volcanic Rocks*, Hobart, Tasmania.

Melosh, H. J., (1996), Dynamical weakening of faults by acoustic fluidization, *Nature*, **397**, 601-606.

Mittempergher, S., G. Di Toro, and G. Pennacchioni, (2007), Effects of fault orientation on the fault rock assemblage of exhumed seismogenic sources (Adamello, Italy), *Geosciences Union Annual Meeting*, Vienna (A) EGU2007-A-05503.

Mizoguchi, K., T. Hirose, T. Shimamoto, and E. Fukuyama, (2007), Reconstruction of seismic faulting by high-velocity friction experiments: An example of the 1995 Kobe earthquake, *Geophys. Res. Lett*., **34**, L01308, doi:10.1029/2006GL027931.

Moecher, D. P. and A. J. Brearley, (2004), Mineralogy and petrology of a mullite-bearing pseudotachylyte: Constraints on the temperature of coseismic frictional fusion, *Am. Mineral*., **89**, 1485-1496.

Moecher, D. P. and Z. D. Sharp, (2004), Stable isotope and chemical systematics of pseudotachylyte and wall rock, Homestake shear zone, Colorado, USA: Meteoric fluid or rock-buffered conditions during coseismic fusion?, *J. Geophys. Res*., **109**, B12206, doi:10.1029/2004JB003045.

Nielsen, S. and J. M. Carlson, (2000), Rupture pulse characterization: Self-healing, self-similar, expanding solutions in a continuum model of fault dynamics, *Bull. Seismol. Soc. Am*., **90**, 1480-1497.

Nielsen, S., G. Di Toro, T. Hirose, and T. Shimamoto, (2008), Frictional melt and seismic slip, *J. Geophys. Res*., **113**, B01308, doi:10.1029/2007JB0051222008.

Obata, M. and S. Karato, (1995), Ultramafic pseudotachylite from the Balmuccia peridotite, Ivrea-Verbano zone, northern Italy, *Tectonophys*., **242**, 313-328.

O'Hara, K., (2001), A pseudotachylyte geothermometer, *J. Struct. Geol*., **23**, 1345-1357.

O'Hara, K. and Z. D. Sharp, (2001), Chemical and oxygen isotope composition of natural and artificial pseudotachylyte: Role of water during frictional melting, *Earth Planet. Sci. Lett*., **184**, 393-406.

Ohtani, T., K. Fujimoto, H. Ito, H. Tanaka, N. Tomida, and T. Higuchi, (2000), Fault rocks and past to recent fluid characteristics from the borehole survey of the Nojima fault ruptured in the 1995 Kobe earthquake, southwest Japan, *J. Geophys. Res*., **105**, 16161-16171.

Ohtomo, Y. and T. Shimamoto, (1994), Significance of thermal fracturing in the generation of fault gouge during rapid fault motion: An experimental verification, *Struct. Geol*., **39**, 135-144 (in Japanese with English abstract).

Okamoto, S., G. Kimura, S. Takizawa, and H. Yamaguchi, (2006), Earthquake fault rock indicating a coupled lubrication mechanism, *eEarth*, **1**, 23-28.

Olsen, K. B., R. Madariaga, and R. J. Archuleta, (1997), Three-dimensional dynamic simulation of the 1992 Landers earthquake, *Science*, **278**, 834-838.

Otsuki, K., N. Monzawa, and T. Nagase, (2003), Fluidization and melting of fault gouge during seismic slip: Identification in the Nojima fault zone and implications for focal earthquake mechanism, *J. Geophys. Res*., **108**(B4), doi:10.1029/2001JB001711.

Passchier, C. W., (1982), Pseudotachylyte and the development of ultramylonite bands in the Saint-Barthelémy Massif, French Pyrenees, *J. Struct. Geol*., **4**, 69-79.

Passchier, C. W. and R. A. J. Trouw, (1996), *Microtectonics*, Springer, Berlin, p. 289.

Pennacchioni, G. and B. Cesare, (1997), Ductile-brittle transition in pre-Alpine amphibolite facies mylonites during evolution from water-present to water-deficient conditions (Mont Mary nappe, Italian Western Alps), *J. Metam. Geol*., **15**, 777-791.

Pennacchioni, G., G. Di Toro, P. Brack, L. Menegon, and I. M. Villa, (2006), Brittle-ductile-brittle deformation during cooling of tonalite (Adamello, Southern Italian Alps), *Tectonophys*., **427**, 171-197.

Philpotts, A. R., (1964), Origin of pseudotachylites, *Am. J. Science*, **262**, 1008-1035.

Philpotts, A. R., (1990), *Principles of Igneous and Metamorphic Petrology*, Prentice Hall, Englewood Cliffs.

Pittarello, L., G. Di Toro, A. Bizzarri, G. Pennacchioni, J. Hadizadeh, and M. Cocco, (2008), Energy partitioning during seismic slip in pseudotachylyte-bearing faults (Gole Larghe Fault, Adamello, Italy), *Earth Planet. Sci. Lett*., **269**, 131-139.

Power, W. L., T. E. Tullis, and J. D. Weeks, (1988), Roughness and wear during brittle faulting, *J. Geophys. Res*., **93**, 15268-15278.

Price, N. J. and J. W. Cosgrove, (1990), *Analyses of Geological Structures*, Cambridge University Press.

Ray, S. K., (1999), Transformation of cataclastically deformed rocks to pseudotachylyte by pervasion of frictional melt: Inferences from clast size analysis, *Tectonophys*., **301**, 283-304.

Reid, H. F., (1910), The mechanism of the earthquake, In: *The California Earthquake of April 18, 1906, Report of the State Earthquake Investigation Commission*, **2**, 1-192, Carnegie Institutions, Washington, D.C.

Reimold, W. U., (1998), Exogenic and endogenic breccias: A discussion of major problematics, *Earth Sciences Reviews*, **43**, 25-47.

B978-0-12-374452-4.00005-2, 00005

Rempel, A. W., (2006), The effects of flash-weakening and damage on the evolution of fault strength and temperature, In: *Earthquakes: Radiated Energy and the Physics of Faulting*, edited by Abercrombie, R., A. McGarr, G. Di Toro, and H. Kanamori, *Geophysical Monograph Series*, **170**, 263-270, American Geophysical Union, Washington, D.C.

Rice, J. R., (1966), Contained plastic deformation near cracks and notches under longitudinal shear, *Int. J. Frac. Mech.*, **2**, 426-447.

Rice, J. R., (2006), Heating and weakening of faults during earthquake slip, *J. Geophys. Res.*, **111**, B05311, doi:10.1029/2005JB004006.

Rowe C. D., J. C. Moore, F. Meneghini, and A. W. McKeirnan, (2005), Large-scale pseudotachylytes and fluidized cataclasites from an ancient subduction thrust fault, *Geology*, **33**(12), 937-940.

Ruina, A., (1983), Slip instability and state variable friction laws, *J. Geophys. Res.*, **88**(B12), 10359-10370.

Sagy, A., E. Brodsky, and G. J. Axen, (2007), Evolution of fault-surface roughness with slip, *Geology*, **35**, 283-286.

Samudrala, O., Y. Huang, and A. J. Rosakis, (2002), Subsonic and intersonic shear rupture of weak planes with a velocity weakening cohesive zone, *J. Geophys. Res.*, **107**, 2170, doi:10.1029/2001JB000460.

Schmid, S. M., H. R. Aebli, F. Heller, and A. Zingg, (1989), The role of the Periadratic Line in the tectonic evolution of the Alps, *Alpine Tectonics*, *Geological Society Special Publication*, *Vol. 45*, edited by Coward M. P., D. Dietrich, and R. G Park, pp. 153-171.

Scholz, C. H., (1998), Earthquakes and friction laws, *Nature*, **391**, 37-42.

Scholz, C. H., (2002), *The Mechanics of Earthquakes and Faulting*, *2nd ed.*, Cambridge University Press, Cambridge, 471 pp.

Scott, J. S. and H. I. Drever, (1953), Frictional fusion along an Himalayan thrust, *Proceedings of the Royal Society of Edinburgh*, *sect. B*, **65**, 121-140.

Shand, S. J., (1916), The pseudotachylyte of Parijs (Orange Free State) and its relation to "trapshotten gneiss" and "flinty crush rock," *Quart. J. Geol. Soc. London*, **72**, 198-221.

Shaw, H., (1972), Viscosities of magmatic silicate liquids; an empirical method of prediction, *Am. J. Sci.*, **272**, 870-893.

Shimada, K., Y. Kobari, T. Okamoto, H. Takagi, and Y. Saka, (2001), Pseudotachylyte veins associated with granitic cataclasite along the Median Tectonic Line, eastern Kii Peninsula, Southwest Japan, *J. Geol. Soc. Japan*, **107**, 117-128.

Shimamoto, T. and H. Nagahama, (1992), An argument against the crush origin of pseudotachylytes based on the analysis of clast size distribution, *Struct. Geol.*, **14**, 999-1006.

Shimamoto, T. and A. Tsutsumi, (1994), A new rotary-shear high-speed frictional testing machine: Its basic design and scope of research, *J. Tectonic Res. Group of Japan*, **39**, 65-78 (in Japanese with English abstract).

Sibson, R. H., (1973), Interactions between temperature and pore fluid pressure during earthquake faulting—A mechanism for partial or total stress relief, *Nature*, **243**, 66-68.

Sibson, R. H., (1975), Generation of pseudotachylyte by ancient seismic faulting, *Geophys. J. Roy. astr. Soc.*, **43**(3), 775-794.

Sibson, R. H., (1977), Fault rocks and fault mechanisms, *J. Geol. Soc. London*, **133**, 191-213.

Sibson, R. H., (1980), Transient discontinuities in ductile shear zones, *J. Struct. Geol.*, **2**, 165-171.

Sibson, R. H., (1989), Earthquake faulting as a structural process, *J. Struct. Geol.*, **11**, 1-14.

Sibson, R. H., (2003), Thickness of the seismic slip zone, *Bull. Seismol. Soc. Am.*, **93**(3), 1169-1178.

Sibson, R. H. and V. Toy, (2006), The habitat of fault-generated pseudotachylyte: Presence vs. absence of friction melt, In: *Earthquakes: Radiated Energy and the Physics of Faulting*, edited by Abercrombie, R., A. McGarr, G. Di Toro, and H. Kanamori, *Geophysical Monograph Series*, **170**, 153-166, American Geophysical Union, Washington, D.C.

Snoke, A. W., J. Tullis, and V. Todd, (1998), *Fault-related Rocks: A Photographic Atlas*, Princeton University Press, New Jersey, 617 pp.

Spray, J. G., (1987), Artificial generation of pseudotachylyte using friction welding apparatus: Simulation of melting on a fault plane, *J. Struct. Geol.*, **9**, 49-60.

Spray, J. G., (1988), Generation and crystallization of an amphibolite shear melt: An investigation using radial friction welding apparatus, *Contrib. Mineral. Petrol.*, **99**, 464-475.

Spray, J. G., (1992), A physical basis for the frictional melting of some rock-forming minerals, *Tectonophys.*, **204**(3-4), 205-221.

Spray, J. G., (1993), Viscosity determinations of some frictionally generated silicate melts: Implications for fault zone rheology at high strain rates, *J. Geophys. Res.*, **98**, 8053-8068.

Spray, J. G., (1995), Pseudotachylyte controversy: Fact or friction?, *Geology*, **23**, 1119-1122.

Spray, J. G., (1997), Superfaults, *Geology*, **25**, 305-308.

Spray, J. G., (2005), Evidence for melt lubrication during large earthquakes, *Geophys. Res. Lett.*, **32**, L07301, doi:10.1029/2004GL022293.

Stesky, R. M., W. F. Brace, D. K. Riley, and P.-Y.F. Robin, (1974), Friction in faulted related rock at high temperature and pressure, *Tectonophys.*, **23**, 177-203.

Stipp, M., H. Stünitz, R. Heilbronner, and S. Schmid, (2002), The eastern Tonale fault zone: A 'natural laboratory' for crystal plastic deformation of quartz over a temperature range from 250 to 700°C, *J. Struct. Geol.*, **24**, 1861-1884.

Stipp, M., B. Fügenschuh, L. P. Gromet, H. Stünitz, and S. M. Schmid, (2004), Contemporaneous plutonism and strike-slip faulting: A case study from the Tonale fault zone north of the Adamello pluton (Italian Alps), *Tectonics*, **23**, TC3004, doi:10.1029/2003TC001515.

Swanson, M. T., (1988), Pseudotachylyte-bearing strike-slip duplex structures in the Fort Foster Brittle Zone, S. Maine, *J. Struct. Geol.*, **10**, 813-828.

Swanson, M. T., (1989), Side wall ripouts in strike-slip faults, *J. Struct. Geol.*, **11**, 933-948.

Swanson, M. T., (1992), Fault structure, wear mechanisms and rupture processes in pseudotachylyte generation, *Tectonophys.*, **204**, 223-242.

Swanson, M. T., (2006), Pseudotachylyte-bearing strike-slip faults in mylonitic host rocks, Fort Foster Brittle Zone, Kittery, Maine, In: *Earthquakes: Radiated Energy and the Physics of Faulting*, edited by Abercrombie, R., A. McGarr, G. Di Toro, and H. Kanamori, *Geophysical Monograph Series*, **170**, 167-179, American Geophysical Union, Washington, D.C.

Takagi, I., K. Goto, and N. Shigematsu, (2000), Ultramylonite bands derived from cataclasite and pseudotachylyte in granites, northeast Japan, *J. Struct. Geol.*, **22**, 1325-1339.

Toyoshima, T., (1990), Pseudotachylite from the Main Zone of the Hidaka metamorphic belt, Hokkaido, northern Japan, *J. Metam. Geol.*, **8**, 507-523.

Tsutsumi, A. and T. Shimamoto, (1997a), High-velocity frictional properties of gabbro, *Geophys. Res. Lett.*, **24**, 699-702.

Tsutsumi, A. and T. Shimamoto, (1997b), Temperature measurements along simulated faults during seismic fault motion, *Proc. 30th Int'l Geol. Congr., Vol. 5*, 223-232.

Tsutsumi, A., (1999), Size distribution of clasts in experimentally produced pseudotachylyte, *J. Struct. Geol.*, **21**, 305-312.

Tullis, T. E., (1988), Rock friction constitutive behavior from laboratory experiments and its implications for an earthquake prediction field monitoring program, *Pure Appl. Geophys.*, **126**, 556-588.

B978-0-12-374452-4.00005-2, 00005

Turcotte, D. L., and G. Schubert, (2002), *Geodynamics*, 2^{nd} *ed*., Cambridge University Press, Cambridge, USA, 472 pp.

Ueda, T., M. Obata, G. Di Toro, K. Kanagawa, and K. Ozawa, (2008), Mantle earthquakes frozen in mylonitized ultramafic pseudotachylytes of spinel-lherzolite facies, *Geology*, **36**(8), 607-610, doi:10.1130/G24739A.1.

Ujiie, K., H. Yamaguchi, A. Sakaguchi, and T. Shoichi, (2007), Pseudotachylytes in an ancient accretionary complex and implications for melt lubrication during subduction zone earthquakes, *J. Struct. Geol*., **29**, 599-613.

Viola, G., N. S. Mancktelow, and D. Seward, (2001), Late Oligocene–Neogene evolution of Europe–Adria collision: New structural and geochronological evidence from the Giudicarie fault system (Italian Eastern Alps), *Tectonics*, **20**, 999-1020.

Wenk, H. R., (1978), Are pseudotachylites products of fracture or fusion?, *Geology*, **l6**, 507-511.

Wenk, H. R., L. R. Johnson, and L. Ratschbacher, (2000), Pseudotachylites in the Eastern Peninsular Ranges of California, *Tectonophys*., **321**, 253-277.

White, J. C., (1996), Transient discontinuities revisited: Pseudotachylyte, plastic instability and the influence of low pore fluid pressure on the deformation processes in the mid-crust, *J. Struct. Geol*., **18**, 1471-1486.

Wibberley. C. A. J, Y., Grabam and G. Di Toro, (2008), Recent advances in the understanding of fault zone internal structure: a review, In: "The Internal Structure of Fault Zones: Implications for Mechanical and Fluid Flow Properties", edited by Wibberley, C. A. J., W. Kurz, J. Imber. R. E. Holdsworth and C. Collettini, *Geological Society Special Publication*, Vol. **299**, 5-33, The Geological Society Publishing House, Bath, UK.

B978-0-12-374452-4.00005-2, 00005

B978-0-12-374452-4.00005-2, 00005

Author Query Form

Book: Fault-Zone Properties and Earthquake Rupture Dynamics
Chapter No:10005

Query Refs.	Details Required	Author's response
AU1	Phrase ok?	